UCLA-ENG-7683
JANUARY 1977

SEISMIC '77

UCLA CONTRIBUTIONS TO THE SIXTH WORLD CONFERENCE ON EARTHQUAKE ENGINEERING

New Delhi, India

The research reported here
was supported in part by the
National Science Foundation

Earthquake Laboratory
Department of Mechanics and Structures
School of Engineering and Applied Science
University of California
Los Angeles, California

50272-101

REPORT DOCUMENTATION PAGE	1. REPORT NO. NSF/RA-770791	2.	3. Recipient's Accession No. PB298270

4. Title and Subtitle
Seismic '77, UCLA Contributions to the Sixth World Conference on Earthquake Engineering

5. Report Date
January 1977

6.

7. Author(s)

8. Performing Organization Rept. No.
UCLA-ENG-7683

9. Performing Organization Name and Address
University of California
School of Engineering and Applied Science
Earthquake Laboratory
Los Angeles, California 90024

10. Project/Task/Work Unit No.

11. Contract(C) or Grant(G) No.
(C)
(G) GI44056
GI44076

12. Sponsoring Organization Name and Address
Engineering and Applied Science (EAS)
National Science Foundation
1800 G Street, N.W.
Washington, D.C. 20550

13. Type of Report & Period Covered

14.

15. Supplementary Notes

16. Abstract (Limit: 200 words)

Nine papers by UCLA Earthquake Laboratory researchers were presented on the following topics: (1) earthquake risk models based on statistical factors of a region; (2) effects of site on ground motion in the 1971 San Fernando earthquake; (3) development of an earthquake risk model based on a bayesian estimate of seismicity; (4) determination of the length of the fault segment which produces significant strong motion at a given location near a very long fault; (5) method of separating body and surface waves in strong motion accelograms and its application to the 1971 San Fernando earthquake; (6) development of a technique to calculate the surface wave transfer functions between two stations; (7) properties of short period surface waves in a layered medium; (8) development of a method of static incremental analysis for predicting collapse of multistory buildings; and (9) use of cyclic cubic test apparatus for liquefaction tests on loose saturated sand.

17. Document Analysis a. Descriptors
Earthquakes
Earthquake resistant structures
Dynamic structural analysis
Seismology
Soil mechanics

b. Identifiers/Open-Ended Terms
Earthquake engineering
San Fernando earthquake
Earthquake risk analysis

c. COSATI Field/Group

18. Availability Statement	19. Security Class (This Report)	21. No. of Pages
NTIS		59
	20. Security Class (This Page)	22. Price PC A04 MF A01

(See ANSI-Z39.18) See Instructions on Reverse

OPTIONAL FORM 272 (4-77)
(Formerly NTIS-35)
Department of Commerce

CAPITAL SYSTEMS GROUP, INC.
6340 EXECUTIVE BOULEVARD
SUITE 25[illegible]
ROCKVILLE, MARYLAND 2[illegible]

CONTENTS

DESIGN EARTHQUAKES BASED ON THE STATISTICS OF SOURCE, PATH AND SITE EFFECTS

by

Kenneth W. Campbell[I]

SYNOPSIS

A method is proposed in which strong earthquake motion and its uncertainty can be predicted from statistical measures of source and propagation characteristics of a region. Three characteristics are used to represent earthquake strong motion: the shape of the power spectral density function, an energy related intensity parameter, and two time domain shaping factors. The risk associated with the estimation of these parameters can be computed from probability and statistical models. Design earthquake motion in the form of accelerograms and response spectra can easily be developed from these parameters for any desired level of risk.

INTRODUCTION

Earthquake risk models proposed to date have concentrated mainly on the random occurrence of earthquakes and have considered only in a preliminary way the uncertainties involved in predicting ground motion. However, several authors have pointed-out the importance of including these uncertainties in seismic risk studies (5, 10, 13).

In an attempt to overcome this deficiency, this study deals with statistically predicting ground motion at a site for an earthquake of a given magnitude and location. The risk associated with the prediction is defined as the probability that the ground motion will be exceeded at a site for the assumed event.

Although much of this work is still in progress, the basic methodology and a brief discussion of the elements of the proposed seismic wave propagation model are presented. Final results and applications will be presented in a later paper.

SYSTEM MODEL

The initiation and transmission of seismic energy in the earth's crust due to an earthquake is a very complex process. However, for engineering purposes it is convenient to model this process with a relatively simple model. Linear system theory has been used as a basis for such a model. The general linear system equation used by Duke and Mal (6) is given by,

$$G = G_B + G_S = E_B W_B X_B + E_S W_S X_S \qquad (1)$$

I Postgraduate Research Engineer, School of Engineering and Applied Science, University of California, Los Angeles.

where

G is the Fourier transform of ground motion
E is the Source Spectrum (Source effects term)
W is the Regional transfer function (propagation effects term)
X is the Local transfer function (site effects term)
B stands for body waves
S stands for surface waves

Because of the great difficulty in separating the relative effects of body and surface waves in strong-motion records, Eq. (1) is simplified to the following form for the purpose of this study,

$$G = EWX \tag{2}$$

where E, W and X are composit transfer functions. Since such a simple model is used to model such a complex process, it is essential that the uncertainties in predicting G from E, W and X be included. Thus, it is suggested that the elements in Eq. (2) be treated as random variables.

CHARACTERIZATION OF STRONG MOTION (G)

The characterization of strong motion should be simple enough to be easily computed, yet sophisticated enough so as to include the important properties of strong earthquake motion. Commonly used indices such as Modified Mercalli Intensity and maximum acceleration have been increasingly criticized for their lack of sensitivity to the duration and frequency distribution of strong motion and are not believed to represent adequately the potential destructiveness of strong motion to man-made structures.

The properties used in this study to characterize strong motion are comprehensive enough so that design motions, such as accelerograms and response spectra, can be easily generated from them. Saragoni and Hart (11) have suggested the following properties: the power spectral density function (PSD), an energy-related intensity parameter, and two time domain shaping factors. From these properties realistic artificial accelerograms can be easily constructed. These properties, then, are used here to characterize strong earthquake motion. They are easily computed from existing digitized accelerograms.

The PSD should be characterized by a small number of points for ease in computations. For this reason it was decided to smooth the PSD in the frequency range 0.14 to 10 hz. (corresponding to periods of 0.1 - 7 sec.), then discretize the smoothed PSD at twenty points. To accomplish this, 10 resolution bandwidths were selected to represent the general level of the PSD for given period ranges of structures, e.g. 0.1 - 0.12, 0.12 - 0.14, etc., with these ranges generally increasing for longer periods. This is consistent with the design philosophy proposed by Blume (3).

The number of points used in the "boxcar" smoothing scheme was determined by the equation,

$$N = \frac{T}{B_e} \tag{3}$$

where T is the record length in seconds used to compute the Fourier transform and B_e is the resolution bandwidth in hertz. A comparison of the

smoothed and raw spectra for several records showed that the smoothed spectra modeled the overall trends in the raw spectra quite well. The randomness in the raw spectra can be modeled from the observation that the deviations between the smoothed and raw spectra divided by the amplitude of the smoothed spectra were found to be uniformly distributed about zero for all frequencies.

SOURCE EFFECTS (E)

The effects of the source have recently become a subject of great concern in engineering seismology. The source displacement spectrum measured in the far field and plotted on a log-log scale has a distinctive shape that can be adequately described by a few parameters (2). This shape is characterized by a flat response at low frequencies, whose amplitude is proportional to seismic moment, and a constant decay rate at high frequencies. The transition between these trends is given by the corner frequency.

Several recent dislocation models (1, 4, 7, 12) suggest the presence of multiple corner frequencies and fault propagation effects in the source spectrum. However, do to limited resolution of observed spectra, these effects are not commonly found and cannot be justifiably included in a study of this scope (16, 17).

Regional differences have recently been shown to be important in modifying the shape of source spectra for events of similar magnitudes (15,16). For instance, earthquakes originating along the California-Nevada border are characterized by significantly smaller seismic moments and higher corner frequencies than those earthquakes originating in the Gulf of California. These regional differences would seem significant enough to be included in the prediction of source parameters.

PROPAGATION PATH EFFECTS (W)

Propagation path effects is a term used to refer to the transmission of seismic energy from the source region to the vicinity of the site. The primary effects are associated with the loss of energy as the seismic waves propagate away from the source region. There are two types of damping that contribute to the loss of energy: geometric attenuation that results from the reduction in energy density as the wave front propagates away from the fault surface, and internal damping due to frictional heat losses.

The distribution of seismic energy within the source region will have a significant effect on the attenuation with distance of strong earthquake motion, especially at near distances for larger earthquakes (9). Therefore, a propagation pattern that takes into account this elongated pattern of energy release along a fault is necessary. This can probably be incorporated in the geometric attenuation term.

A model commonly used to model the loss of energy due to internal damping is given by,

$$A(\omega) = A_0(\omega) \exp(-\omega r/2QV) \qquad (5)$$

where $A(\omega)$ is the spectrum at the source, ω is circular frequency, r is distance from the source, Q is a material damping factor, and V is the

seismic velocity of the medium.

SITE EFFECTS (X)

Site effects is a term used to describe the modification of strong motion within the vicinity of the site. Several studies have shown that various types of site conditions have a significant effect on the recorded motion at a site. Most significant for this study are the studies of Hayashi et. al. (8) and Seed et. al. (14), which demonstrated differences in the shapes of earthquake response spectra for various site classes. These site classes consisted of sites grouped as to the firmness and depth of their overburden soils.

Since the PSD spectrum covers a broad frequency range, those factors affecting the short period portion of the spectrum would not be expected to be the same as the factors affecting the long period portion. Therefore, a site classification scheme should necessarily be flexible. For instance differences in the upper 50 feet or so of a soil deposit probably most significantly affect the short period portion of the spectrum, whereas, the depth to basement rock may be the controlling factor in the long period range.

The final result would be a relatively comprehensive set of geotechnical classifications. Each classification would be represented by amplification spectrum giving the expected increase in the discretized PSD at each frequency point over that of some reference group.

CONCLUSION

A basic methodology has been presented herein that briefly describes a model for predicting ground motion from the models of three important elements of the system: source, propagation and site effects. However, much more work is required to impliment the method. Models for each effect must be more fully developed and probability models must be incorporated in order to introduce uncertainty into the procedure. All available strong motion data will be used to formulate and calibrate these models.

In its final form, the model can be used to develop design ground motions, for a specified level of risk, in the form of power spectral densities, artificial accelerograms, and response spectra. When combined with a model of the random occurrence of earthquakes in space, time and magnitude (5) one would have available a means of predicting a comprehensive measure of strong motion, which takes into account all the uncertainties involved in modeling the occurrence and transmission of strong earthquake motion.

BIBLIOGRAPHY

1. Aki, K. (1973). Scaling Law of Earthquake Source Time-Function, Geophys. J., Vol. 31, 3-25.

2. Bath, M. (1974). Spectral Analysis in Geophysics, Elsevier Scientific Publishing Company, Amsterdam.

3. Blume, J.A. (1970). An Engineering Intensity Scale for Earthquake and Other Ground Motion, Bull. Seism. Soc. Am., Vol. 60, 217-229.

BIBLIOGRAPHY (cont.)

4. Brune, J.N. (1970). Tectonic Stress and the Spectra of Seismic Shear Waves from Earthquakes, J. Geophys. Res., Vol. 75, 4997-5009.

5. Cornell, C.A. and E.H. Vanmarcke (1969). The Major Influences on Seismic Risk, Proc. 4th World Conf. Earthq. Engr., E.E.R.I., 17-24.

6. Duke, C.M. and A.K. Mal (1975). A Model for Analysis of Body and Surface Waves in Strong Ground Motion, Proc. U.S. Natl. Conf. Earthq. Engr., E.E.R.I., 17-24.

7. Haskell, N.A. (1966). Total Energy and Energy Spectral Density of Elastic Wave Radiation from Propagating Faults, Part II, A Statistical Source Model, Bull. Seism. Soc. Am., Vol. 56, 125-140.

8. Hayashi, S., H. Tsuchida, and E. Kurata (1974). Average Response Spectra for Various Subsoil Conditions, Third Joint Meeting, U.S.-Japan Panel on Wind and Seismic Effects, UJNR, Tokyo.

9. Housner, G.W. (1970). Strong Ground Motion, in Earthquake Engineering, Prentice-Hall, 75-91.

10. Newmark, N.M., A.R. Robinson, A.H.-S. Ang, L.A. Lopez, and W.J. Hall (1972). Methods for Determining Site Characteristics, Proc. Microzonation Conf., Vol. I, 113-129.

11. Saragoni, G.R. and G.C. Hart (1972). Nonstationary Analysis and Simulation of Earthquake Ground Motions, Earthq. Engr. and Structural Laboratory, Univ. of California, Los Angeles, UCLA-ENG-7238.

12. Savage, J.C. (1972). Relation of Corner Frequency to Fault Dimensions, J. Geophys. Res., Vol. 77, 3788-3795.

13. Seed. H.B. (1974). Site Effects in Earthquake-Resistant Design, Proc. 1st Venezuelian Conf. on Earthq. Engr.

14. Seed, H.B., C. Ugas, and J. Lysmer (1974). Site-Dependent Spectra for Earthquake-Resistant Design, Earthq. Engr. Res. Center, Univ. of California, Berkeley, EERC 74-12.

15. Thatcher, W. (1972). Regional Variations of Seismic Source Parameters in the Northern Baja California Area, J. Geophys. Res., Vol. 77, 1549-1565.

16. Thatcher, W. and T.C. Hanks (1973). Source Parameters of Southern California Earthquakes, J. Geophys. Res., Vol. 78, 8547-8576.

17. Tucker, B.E. and J.N. Brune (1973). Seismograms, S-Wave Spectra, and Source Parameters for Aftershocks of San Fernando Earthquake, in San Fernando, California, Earthquake of February 9, 1971, NOAA-EERI, Vol. III, 69-121.

Sixth World Conference
on Earthquake Engineering,
New Delhi, 1977

EFFECTS OF SITE ON GROUND MOTION IN THE SAN FERNANDO EARTHQUAKE

C. M. Duke, R. T. Eguchi, K. W. Campbell and A. W. Chow[I]

SYNOPSIS

Basement and free field accelerograph stations that recorded the San Fernando, California earthquake of February 9, 1971 were compared with geological and geophysical site data, particularly shear wave velocity profiles. Geophysical surveys were made at 47 accelerograph sites to determine the velocity profiles to about 70 feet in depth.

Both peak particle velocity and Arias instrumental intensity were found to have statistically significant dependence upon the mean shear wave velocity and the rate at which it increased with depth.

INTRODUCTION

A relationship between local site conditions and ground motion has been reported for almost every large magnitude earthquake throughout the world. Measures of the ground motion aspect of this relationship have been until recently limited to the qualitative. However, in the 1971 San Fernando earthquake there were obtained a large number of strong motion accelerograms corresponding with a variety of local site conditions. Various authors have studied the peak indices of these instrumental data, but a clear cut relation between shaking and site conditions has continued to elude recognition.

Attention therefore was transferred to quantitative dynamic representations of the site conditions, with the thought that such a representation might lead to better correlation than the largely static and qualitative representations used in the past, such as surface geology, good vs. bad soil, and depth of alluvium.

One quantitative indicator of the dynamic character of a site is the profile of seismic shear wave velocity as a function of depth down to approximately 70 feet. As will be shown, use of this representation facilitates a statistically significant correlation with certain indices of strong motion in the San Fernando earthquake. This correlation is the focus of this paper (1).

Granted that strong earthquakes generate higher strain level shear velocities than those measured with geophysical seismic techniques, it is nevertheless possible that a correlation could exist. Use of the shear velocity profile would appear to bring in the influences of both body and surface wave responses at a site. Of course, other factors such as source mechanism, directionality and deeper subsurface geology should also be expected to affect any correlation of site conditions with ground motion.

[I]Department of Mechanics and Structures, University of California, Los Angeles, California.

Shallow refraction surveys (2,3) were made at or near to 47 stations which had recorded the San Fernando earthquake at or near to the ground surface. The accelerograph data were furnished by the U. S. Geological Survey after processing by California Institute of Technology (4).

ANALYSIS

The ground motion parameters used were the peak values of acceleration, velocity and displacement, and the value of Arias Intensity, designated A, V, D and I_a, respectively. Arias intensity is a measure of the area under the power spectral density graph of acceleration (5). The values of A, V and D adopted for analysis were the highest peaks obtained from the corresponding time history plots, considering both horizontal records at the site. The I_a value used was the sum of the intensities in the two horizontal directions.

The parameter of the shear wave velocity profile was obtained from the fact that shear wave propagation velocity, here called β, increases with a power, n of the depth, d:

$$\beta = Kd^n = Kd^{0.37} . \qquad (1)$$

The value of 0.37 for n was found (6) to represent very well the variety of Los Angeles area soils down to 100 feet or so of depth, and was therefore used. This leaves K, a constant, as the site parameter.

Examples of K values are shown in Figure 1. K was obtained for each site by least squares fitting of the results of refraction surveys, using the circled points and the origin, Figure 2. As will be shown, K values correlate rather well with certain ground motion indices for sites on soil, but do not correlate for rock outcrop sites. For rock sites the lithology of the rock may be used instead, but with only rough fitting.

The first result is in Figure 3, showing peak velocity. It was found that the soil sites generally fell into one of two categories: those that experienced higher ground motion tended to have greater K values than sites that experienced lower ground motion. Numerical values of K shown on the figure correspond with the separations of the soil sites into two classifications. It is seen from the figure, as well as from the statistical coefficients in Table 1, that these separations of soil sites are quite pronounced when either V or I_a is the strong motion index.

The rock sites were classified as either sedimentary or basement complex (igneous and metamorphic), according to the surface geology. The correlations are less significant than for the soil sites.

Peak acceleration and displacement did not reveal significant correlations for either soil or rock sites and therefore have been left out of this paper, except that the coefficients are given in Table 1.

Encouraged by certain of these correlations for soils, the computation was made of multiple regressions of peak particle velocity on distance and K value, Figure 4. This was also done for Arias intensity, Figure 5. Table 2

presents the statistical coefficients. These correlations in continuous rather than inequality form may be adaptable for engineering use. Figures 4 and 5 apply for soil sites only. Again it was found that peak acceleration and displacement were only poorly correlated with K.

APPLICATION

As an example of practical use of the results, imagine a site on soil with established K, located at a known distance from an earthquake of magnitude 6.4 (e.g., the 1971 San Fernando Earthquake). Use the multiple regression of Figure 4 to establish the peak particle velocity of ground motion predicted for the site.

Should one wish to have the output in terms of peak acceleration instead of peak velocity, use could be made of the tripartite logarithmic graph with relative ground motion values of A = 1.0g, V = 48 in/sec. and D = 36 in. (7).

Values of K for such an application may be determined from shear wave velocity profiles, using either field or laboratory measurements or a simulation procedure (6).

The quality of the correlations presented would seem to warrant similar studies of future earthquakes that yield large amounts of instrumental data.

ACKNOWLEDGMENT

Thanks are extended to the National Science Foundation for financial support of this research, under Grant GI 44056.

BIBLIOGRAPHY

1. Duke, C. M., R. T. Eguchi, K. W. Campbell and A. W. Chow, "Effects of Site on Ground Motion in the San Fernando Earthquake," Report UCLA-ENG, University of California, Los Angeles, 1976.

2. Duke, C. M., J. A. Johnson, Y. Kharraz, K. W. Campbell and N. A. Malpiede, "Subsurface Site Conditions and Geology in the San Fernando Earthquake Area," Report UCLA-ENG-7206, University of California, Los Angeles, 1971.

3. Eguchi, R. T., K. W. Campbell, C. M. Duke, A. W. Chow and J. Paternina, "Shear Velocities and Near-Surface Geologies at Accelerograph Sites that Recorded the San Fernando Earthquake," Report UCLA-ENG-7653, University of California, Los Angeles, 1976.

4. California Institute of Technology, "Strong Motion Earthquake Accelerograms, Digitzied and Plotted Data," Vol. II, 1971-1975.

5. Arias, Arturo, "A Measure of Earthquake Intensity," Proc. Conf. Seismic Design Nuclear Power Plants," Massachusetts Institute of Technology, pp. 438-483, 1970.

6. Campbell, K. W. and C. M. Duke, "Correlations among Seismic Velocity, Depth and Geology in the Los Angeles Area," Report UCLA-ENG-7662, University of California, Los Angeles, 1976.

7. Newmark, N. M. and W. J. Hall, "A Rational Approach to Seismic Design Standards for Structures," Proc. 5th World Conf. on Earthquake Engr., Rome, Italy, 1973.

TABLE 1

STATISTICAL COEFFICIENTS FOR FIGURE 3

Index	K Separation	Correlation Coefficient
Peak Velocity	$K \leq 490$	0.98
	$K > 490$	0.90
Arias Intensity	$K \leq 490$	0.87
	$K > 490$	0.91
Peak Acceleration	$K \leq 450$	0.62
	$K > 450$	0.89
Peak Displacement	$K \leq 475$	0.75
	$K > 475$	0.52

TABLE 2

STATISTICAL COEFFICIENTS FOR FIGURES 4 AND 5

Index	Correlation Coefficient
Peak Velocity	0.90
Arias Intensity	0.86
Peak Acceleration	0.71
Peak Displacement	0.59

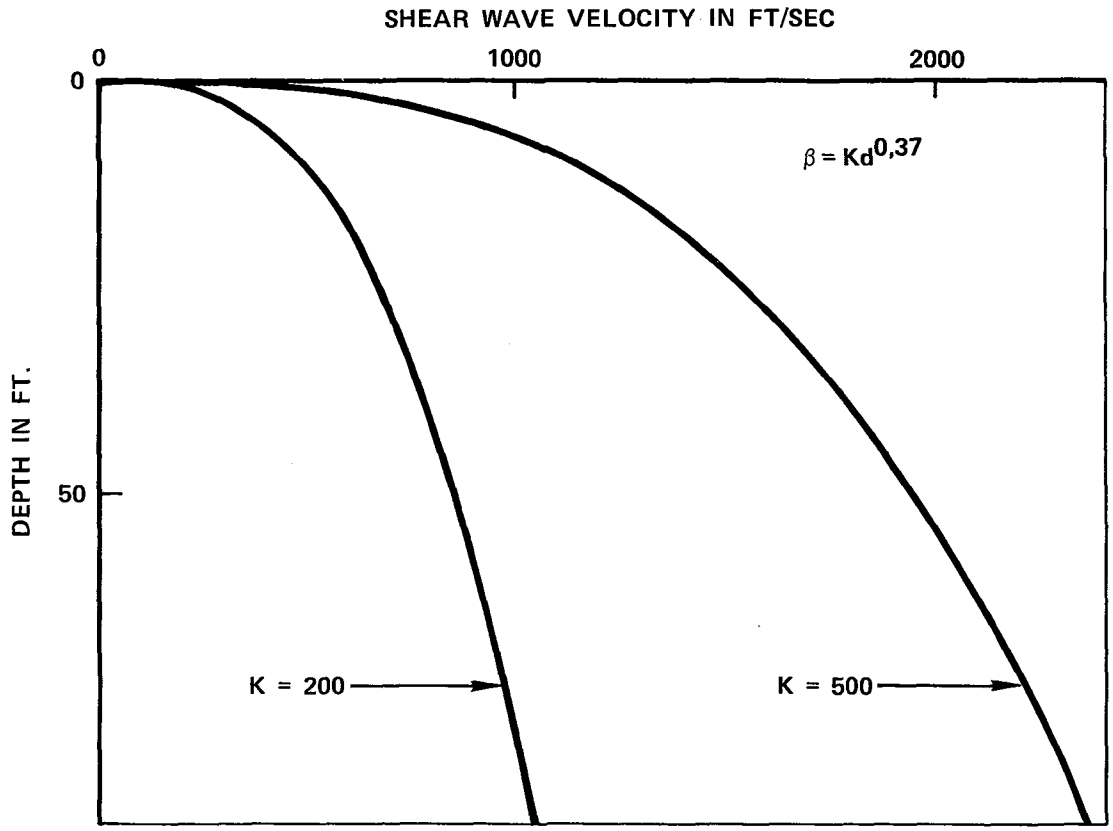

Figure 1. Dependence of Shear Wave Propagation Velocity on Depth and K Value.

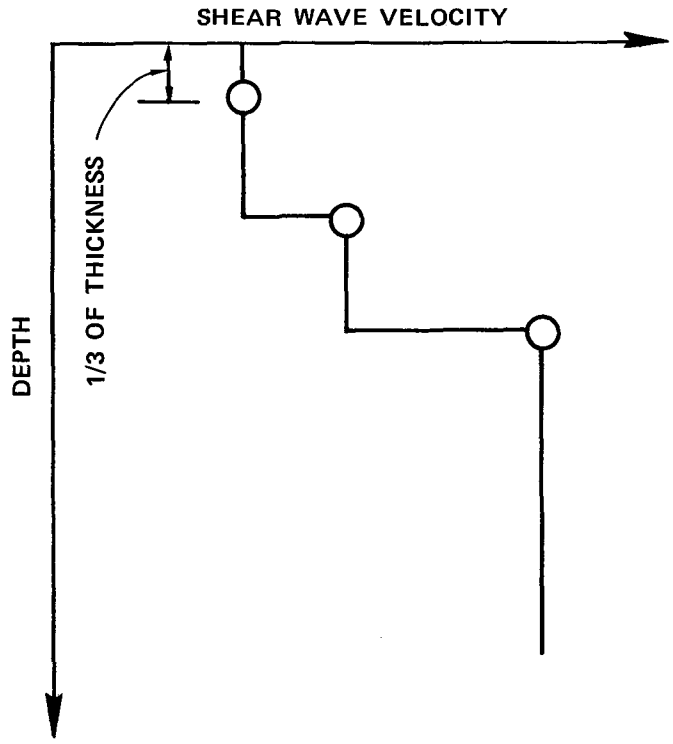

Figure 2. Method of Determining Shear Wave Velocity Profile from Refraction Survey.

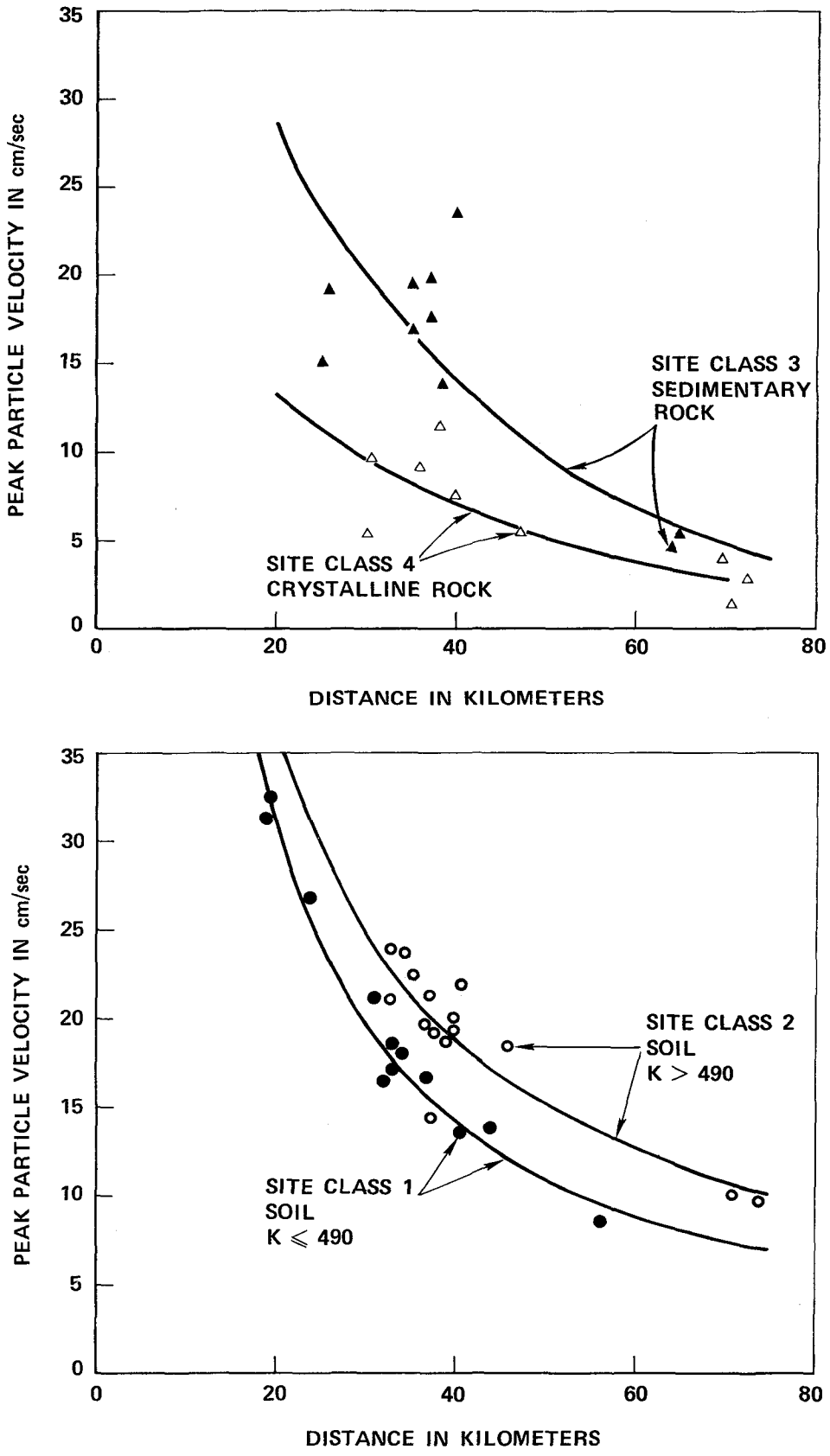

Figure 3. Attenuation of Peak Particle Velocity for Soil and Rock Site Classifications

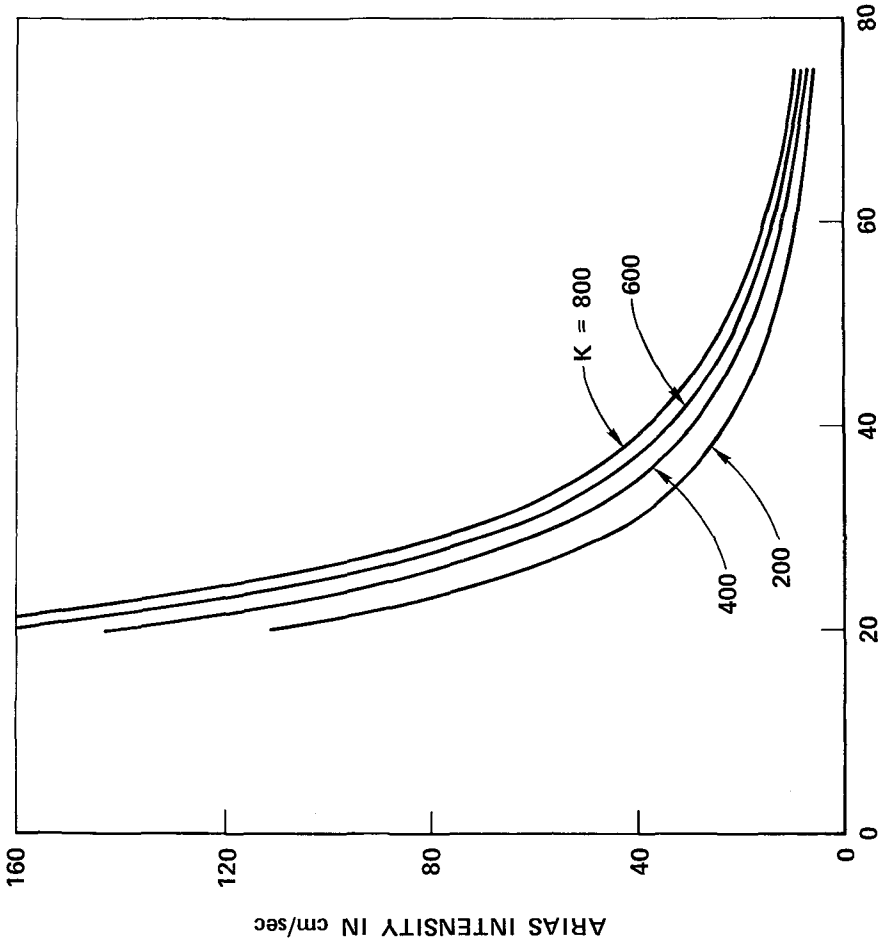

Figure 5. Multiple Regression of I_a on R and K.

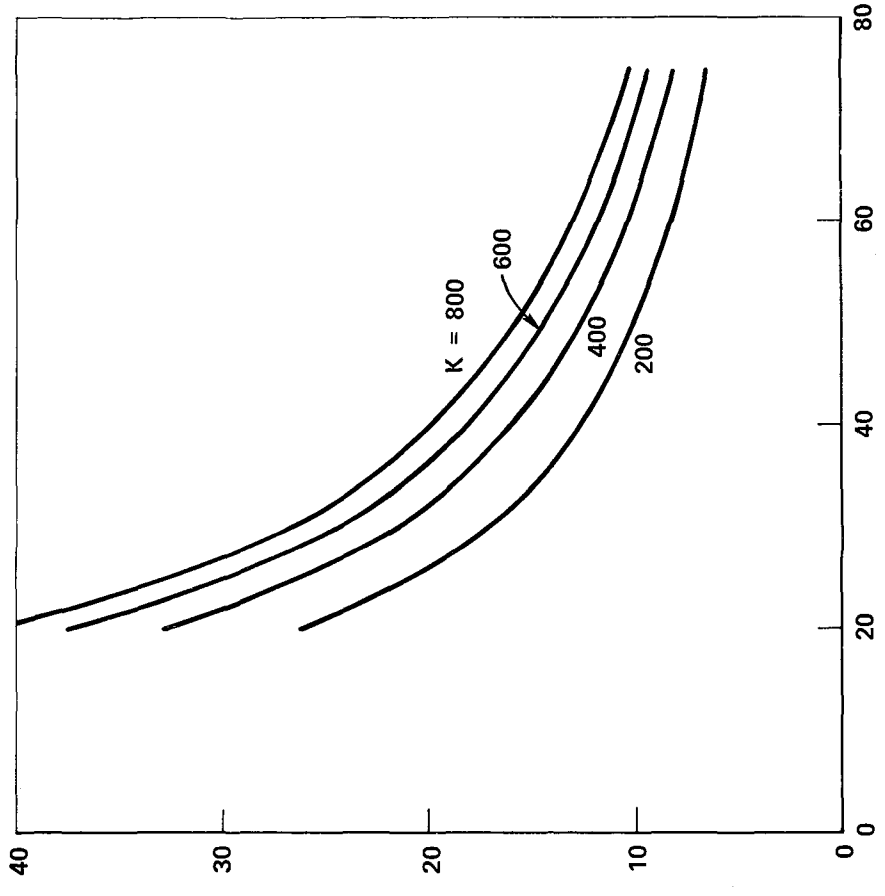

Figure 4. Multiple Regression of V on R and K.

SEISMICITY AND SITE EFFECTS ON EARTHQUAKE RISK

by

Ronald T. Eguchi[I] and Kenneth W. Campbell[II]

SYNOPSIS

An earthquake risk model that incorporates a bayesian estimate of seismicity and an amplification factor for local site conditions is developed and applied to the Los Angeles, California area. Recency of faulting is used as a criteria for assigning activity rates to faults with no "historic" record of earthquake epicenters. Shear-wave velocity profiles are used to characterize local site conditions. 100-year expected peak velocities are computed by combining the above models with probability and statistical models of earthquake occurrence.

INTRODUCTION

Decisions of the routing of aqueducts, transportation, and electric power transmission systems in seismically active regions should incorporate a consideration of the risk of seismic shaking along the various possible routes. In regions such as California, where the seismic regime and areal geology are comparatively well understood, it is useful for this purpose to display the seismic risk of the region on maps. This paper outlines a methodology for estimating these risks, and applies the method to a part of the Los Angeles area. Risk, as it is used throughout this paper, is defined as the probability that a ground motion index (such as peak velocity) will be exceeded within a certain period of time for a specified design life.

The main features of the present paper are the utilization of a bayesian-type seismicity model and the incorporation of a quantitative site effects model. The former represents an attempt to utilize geologic data, such as recency of faulting, to estimate the activity of major faults having no "historic" earthquake epicenters associated with them. The site amplification model includes the effect of local site conditions on the intensity of seismic shaking. As a result, a site classification scheme, based on the utilization of shear-wave velocity profiles, is presented and is incorporated into the analysis of risk.

SEISMICITY

Since the historic record of earthquake occurrences in Southern

---

I Research Engineer, J.H. Wiggins Company, Redondo Beach, California, formerly Postgraduate Research Engineer, School of Engineering and Applied Science, University of California, Los Angeles.

II Postgraduate Research Engineer, School of Engineering and Applied Science, University of California, Los Angeles.

California is of relatively short length and subject to large uncertainty (2), it was decided to use both historic seismicity data as well as regional tectonics to assess the activity of the major faults of the region.

Thirty-five faults within a 200-kilometer radius of the study zone were selected as potential sources of future earthquakes, Fig. 1. The faults were grouped into three classifications based on their known recency of activity and surface faulting (1): these being active (A), potentially active of high potential (HP), and potentially active of low potential (LP). A fourth group classified as inactive (IA) by the A.E.G. criteria was excluded from consideration. This classification is believed to give a reasonable indication of the relative amounts of seismic activity that can be expected in the future (4).

The historical seismicity of the 200-kilometer region surrounding the site was determined from available catalogs of Southern California earthquakes occurring from 1812 through 1975. Based on this data, the recurrence curve for the region was found to be,

$$\text{Log}_{10}N = 5.34 - 1.0M \qquad (1)$$

where N is the number of events per year occurring within the region having Richter magnitude M or greater. The San Jacinto Fault was the only fault for which enough historical data was available to establish a recurrence curve. This curve, established for a narrow zone surrounding a 266-kilometer segment of the fault is given by,

$$\text{Log}_{10}N = 3.82 - 0.79M \qquad (2)$$

The lack of adequate historical activity to establish recurrence curves for the remaining faults requires some sort of "bayesian" assessment of their activity rates. In this respect it was assumed that each fault classification could be characterized by a constant activity rate per unit length of fault. This, of course, excludes the San Jacinto Fault whose activity is given by Eq. (2). Active faults were assigned an activity rate per unit length based on the historic seismicity of the region, Eq. (1), less the seismicity associated with the San Jacinto Fault. This conservatively assigns all of the past historic activity to those known active faults. HP-type and LP-type faults were arbitrarily assigned activity rates per unit length of 1/2 and 1/6 times that of the active faults. The values of 1/2 and 1/6 represent preliminary estimates and should be revised accordingly as research warrants. The b-value, or slope of the recurrence curve, for each fault classification was given a value of -1.0 as established for the region as a whole.

LOCAL SITE CONDITIONS

An important concern to those estimating earthquake risk is the effect of local site conditions on expected earthquake ground motions. In the past only limited correlations between qualitative site classifications and various instrumental indices have been found. Recently, however, a new classification system was introduced which uses a quantitative representation of site properties to characterize site effects (3). The technique consists of fitting parabolic functions through shear-wave velocity profiles using the following equation,

$$V_s = Kd^{0.37} \quad (3)$$

where V_s is shear wave propagation velocity (ft/sec); d is depth (ft); and K is a constant. Therefore, the dependence of velocity on depth can be established by the value of K.

Using K to represent a measure of site properties, multiple regression (3) were performed using ground motion index data provided by the 1971 San Fernando earthquake. From this analysis, a strong correlation was found between peak particle velocity, V (cm/sec), and K. This relationship, as a function of hypocentral distance R in kilometers, is given below and in Fig. 2,

$$V = e^{4.69}K^{.33}R^{-1.05} \quad (4)$$

Correlations utilizing peak acceleration and peak displacement exhibited little dependence on K. In order to incorporate magnitude into the analysis, Eq. (4) was multiplied by $e^{1.2(m-6.4)}$.

Equations similar to Eq. (4) were also established for two types of rock: Sedimentary and Basement Rock. These equations, however, do not incorporate K-values.

PROBABILITY DISTRIBUTION

The joint probability distribution utilized to represent the occurrence of earthquakes in time, magnitude and space was a Gumbel Type II extreme value distribution. This distribution, transformed to give the distribution of maximum annual peak velocity using Eq. (4), is given by,

$$P(V>v) = 1-e^{-t/T} \quad (5)$$

where P(V>v) is the probability that peak velocity is exceeded (i.e. risk) in t years; t is the design life of the structure under consideration, and T is the return period. For specified values of risk, design life and return period, the design peak velocity can be computed by an iterative solution of Eq. (5).

For the purpose of this study, the following parameters were used; T = 100 years, t = 50 years, and risk = 0.39.

EXAMPLE

To illustrate the methodology, an example is presented using a part of the Los Angeles area. The Basement and Sedimentary rock estimates of 100-year peak velocities is given in Fig. 3. Geographically, the rock sites are located in the top portion of the study area. In general, the velocities exhibit little variation within each of the two rock groups.

The soil site estimates of velocity in Fig. 3, however, have been computed using a reference K-value of 400. Because of this, the variation in values can be attributed totally to effective fault distances. Note that the largest value of velocities lie diagonally on a line from the lower right-hand corner to the upper left-hand corner of Fig. 3. This trend is due to the presence of the Newport-Inglewood fault.

Since the 100-year velocities for the soil sites were computed using a reference K-value, a velocity coefficient is used to obtain the site-dependent velocities. This coefficient, C_v, is computed from the following equation,

$$C_v = (K/400)^{.37} \qquad (6)$$

where K represents the soil parameter determined from the shear-wave velocity profile. The base soil velocity, V_{400} is then multiplied by this coefficient to obtain the expected velocity, V_k, for the site.

By incorporating C_v, the site velocities, V_k, for the three sites are found to vary from 33 to 45 cm/sec. The original base velocities, however, only span a 3 cm/sec range. The rock velocities range from 13 cm/sec for Basement Rock to 27 cm/sec for Sedimentary Rock. Therefore, for this example, K-value and rock type have a greater effect on the areal distribution of velocity than does the seismicity of the region.

CONCLUSION

A method of computing the 100-year design ground motion for a site is presented and applied to a portion of the Los Angeles area. The important features of the method include 1) a bayesian assessment of fault activity rates and 2) a quantitative assessment of site effects. For the relatively small study area used in this paper, it was observed that site conditions had a much greater effect on the 100-year velocities than did the regional seismicity. However, with the inclusion of a larger study area, the effect of seismicity would be expected to become more significant.

BIBLIOGRAPHY

1. AEG (1973). Geology and Earthquake Hazards, Planners Guide to the Seismic Safety Element, Association of Engr. Geologist, So. California Section.

2. Allen, C.R. (1975). Geological Criteria for Evaluating Seismicity, Bull. Geol. Soc. Am., Vol. 86, 1041-1057.

3. Duke, C.M., R.T. Eguchi, K.W. Campbell and A. Chow (1976). A Site Classification for Strong Motion Analysis, Proc. 6th World Conf. Earthq. Engr., New Delhi, India.

4. Ziony, J.I., C.M. Wentworth, and J.M. Buchanan (1973). Recency of Faulting; A Widely Applicable Criterion for Assessing the Activity of Faults, Proc. 5th World Conf. Earthq. Engr., 1680-1683.

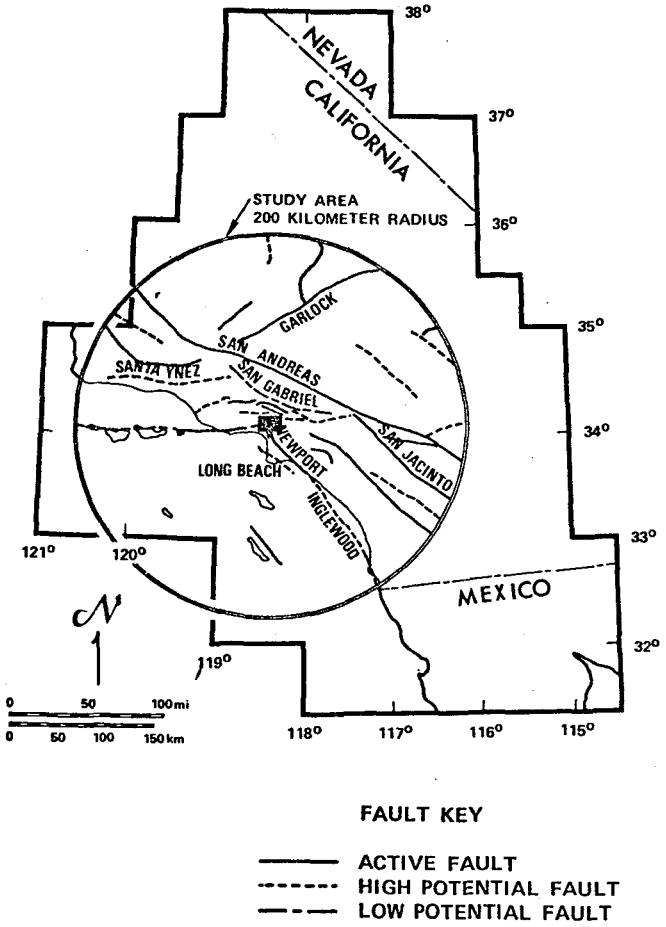

Figure 1. Base Fault Map for Southern California.

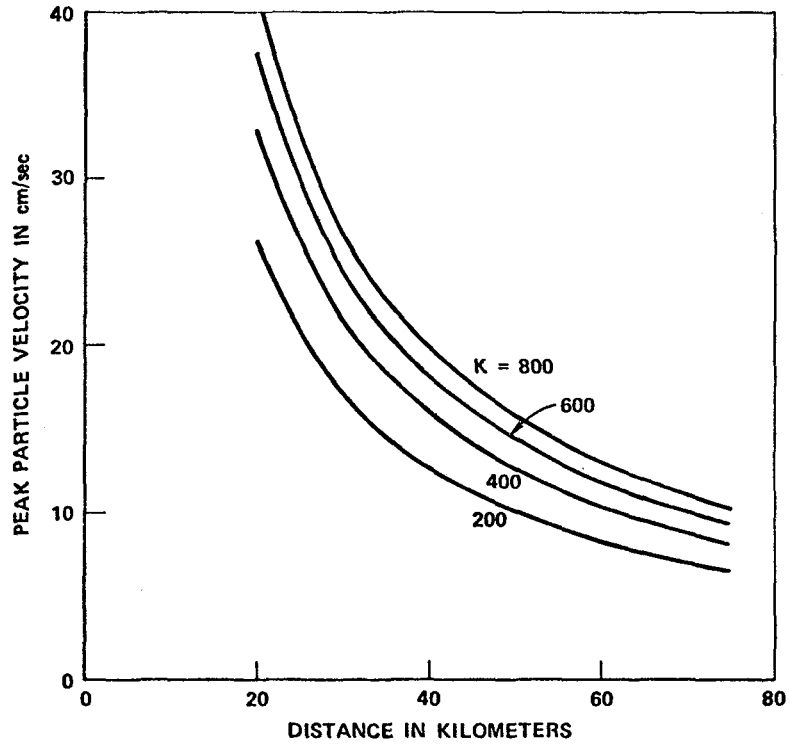

Figure 2. Multiple Regression of Peak Velocity on Hypocentral Distance and K-Valve.

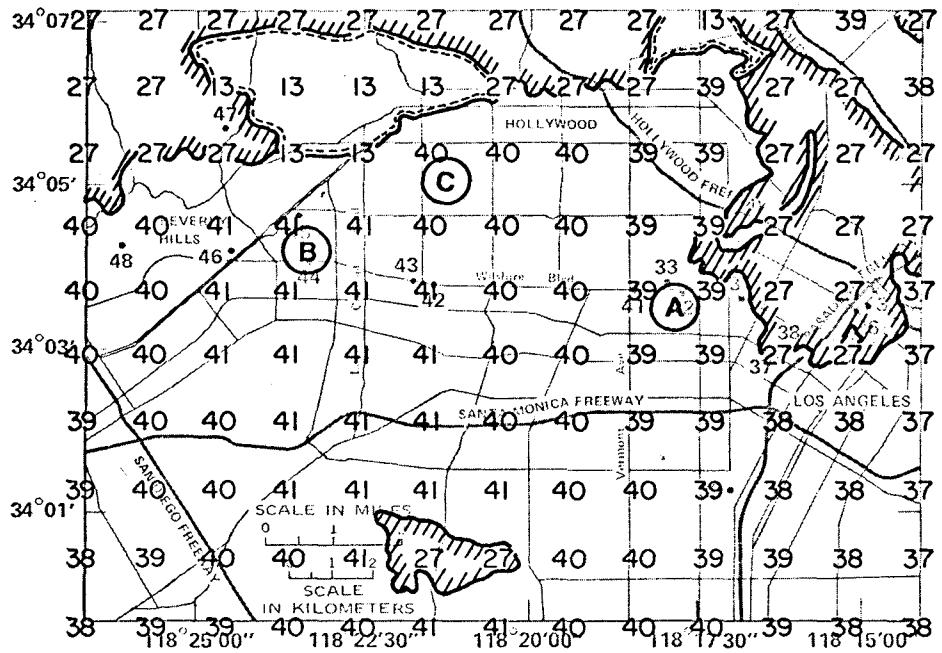

KEY

40	100 YEAR VELOCITY		BASEMENT ROCK
	SEDIMENTARY ROCK		SOIL (K = 400)

Figure 3. 100–Year Velocity Base Map for Central Los Angeles.

TABLE 1
COMPUTATION OF 100-YEAR PEAK VELOCITY

SITE	LOCATION	K-VALUE	V_{400} (cm/sec)	C_v	V_k (cm/sec)	M.M.I.
A	616 S. NORMANDIE, L.A.	603	39	1.15	45	IX
B	435 OAKHURST, BEVERLY HILLS	429	41	1.02	42	IX
C	1100 HIGHLAND, HOLLYWOOD	231	40	0.83	33	VIII–IX

THE INFLUENCE OF SOURCE PARAMETERS ON STRONG GROUND MOTION

by

N.A. Levy[I] and A.K. Mal[II]

SYNOPSIS

Near field ground motions are calculated from a rapidly propagating vertical fault located in a homogeneous isotropic visco-elastic half space. A model of the source is constructed by retaining the essential kinematic features of the faulting process. Synthetic displacements and velocities are calculated by means of an efficient computer program. The influence of the rupture speed on the nature of the ground motion is investigated by varying the speed between the Rayleigh and the P wave speed of the medium. The differences in the nature of the motions produced by strike-slip and dip-slip faultings of equal seismic moments are studied. The relative magnitudes of the body waves and the surface waves in near field motions are compared. An effort is made to determine the length of the fault segment which produces the significant strong motion at a given location near a very long fault.

INTRODUCTION

The problem of the calculation of near field ground motion from shallow earthquakes has received much attention in recent years. The major goal in these studies has been the prediction of displacement, velocity and acceleration of the ground at a given location under assumed motion at the source.

In strong ground motion calculations, reasonable models of the earthquake source and the earth in the vicinity of the source must be constructed. Since the source has a strong influence on the near field motion, an accurate model of the source must necessarily be employed. Unfortunately, the mechanics of the earthquake source is not very well understood at the present time. It has been established, however, that almost all shallow earthquakes are caused by propagating ruptures along preexisting fault surfaces. Thus, a reasonable model of the source must, at least, be consistent with the theories of fracture. The model of the ground should, in principle, be a multilayered medium containing all the discontinuities in the physical properties. Since the free surface represents the strongest discontinuity in the earth's crust, a uniform half space may serve as a reasonable exploratory model of the ground. This should account for some of the major features (e.g. reflection, surface waves) expected to be present in the ground motion. In addition, the method of analysis must be flexible enough so that the significant results of current research on fault dynamics (such as the influence of ambient

[I]Mathematician, U.S. Naval Undersea Research Center, San Diego, California 92132.

[II]Professor, Department of Mechanics and Structures, University of California, Los Angeles, California 90024.

tectonic stress, friction, etc.) may be included, as they become available. It should also be adaptable to multilayered media.

All the models considered in the literature so far are over-simplified in that they ignore one or more of the essential ingredients described above, (see, e.g. [1] and [2] for a review of the earlier work). Some of these authors were able to obtain reasonable agreement between theoretically computed ground displacements and the displacements obtained by integrating the near field accelerations recorded in two earthquakes (Parkfield 1966, San Fernando 1971). Since the inversion procedure involved in the comparison is highly non-unique, it is difficult to determine the effectiveness of their techniques for prediction purposes.

In a recent paper [3] an alternative theoretical basis was presented by retaining all of the ingredients discussed above. The technique was applied to calculate the ground displacements in the vicinity of the fault in a simplified model of the 1966 Parkfield (California) earthquake. The agreement between the predicted and recorded motion was quite good. The results presented in the present paper are based on the theory developed in [3] and are of general interest in engineering seismology.

RESULTS

We consider a vertical dip-slip or strike-slip fault of relatively small width and shallow depth - buried in a uniform half space (Fig. 1). The rupture is assumed to begin at the hypocenter H, spread rapidly through the width b and propagate unilaterally (to the right) along the rectangular fault surface. The slip across the rupture surface is assumed to vary nonuniformly between a zero value at the edge and a maximum value at the center. The maximum static offset in either dip-slip or strike-slip case is D at the center of the rectangle (a x b) swept by the rupture surface. In the numerical calculations the source parameters were assigned the values, d = 3 km., a = 30 km., b = 6 km., D = 3 m. The medium was assumed to be homogeneous and isotropic with the properties $c_1 = \sqrt{3}c_2 = 5.6$ km/sec., $c_r = 2.9$ km/sec., where c_1, c_2, c_r are the velocities of the P, S and Rayleigh waves respectively. The damping properties of the medium were realized by assigning an imaginary part to the velocities with the attenuation coefficients $Q_p = Q_s = 50$. The recording station was assumed to be located at a point halfway across the fault surface at a distance equal to the fault length.

The influence of the variation of the rupture speed c ($c_r < c < c_1$) on the calculated displacement and velocity time histories are shown in Figures 2 and 3 respectively. The DC components of the ground motion were removed by a low frequency cut-off of .07 Hz. A high frequency cut-off of 3 Hz was used for the displacements and 6 Hz for the velocities. No appreciable energy was present beyond these frequencies. The time histories were shifted in time by assuming that the motion at the station was initiated by the P wave arrival. Only the displacement components perpendicular to the fault surface are shown in the figures, the effect is similar in the other components. The major feature in these curves is the growth of the peak displacements and velocities with increasing rupture speed, especially in the dip-slip case. It should also be noted that in the strike-slip case, the peak velocity shows no significant increase except when the rupture speed is very close to the P wave speed.

In Figures 4a and 4b, the amplitudes of the body wave and Rayleigh wave displacement spectra are compared for a fixed rupture velocity of 2.9 km/sec. The notable aspect of these curves is the predominance of body wave motion in the strike-slip case and Rayleigh wave motion in the dip-slip case. This suggests that surface waves would be of considerable interest in earthquakes stemming from a rupture surface with a strong dip component. It should also be noted that the vertical displacement is of the same order for both strike-slip and dip-slip. One other somewhat unexpected feature is the relative peak in the parallel strike component at the higher frequencies. The fact that it appears in the 1 Hz region may have some bearing on the previous oscillatory behavior in the same component's time history (Figs. 2, 3).

The possibility of simplifying near-field ground motion calculations was examined by computing displacement spectra from the strike-slip case by using only portions of the rupture surface, comparing these to the results obtained using the entire fault surface. The hypothetical recording station was positioned half way along the fault, at a distance of a/2 from the fault surface and contributions from symmetric portions of the fault surface with respect to the recording station were calculated. It is to be noted that the important features of the motion begin to emerge for the case where the fault segment length is equal to the station distance. The most pronounced change is observed in the perpendicular and vertical components, and can be attributed to the proportionately smaller contribution of the tangential dislocation for the shorter fault segments. The effect of successively larger fault segments appears as attenuation of the higher frequencies, as might be expected from the longer period motion generated from increasing fault size. The results for the nearer station located one quarter fault length in perpendicular distance were very similar (not shown). Only in this case the essential ground motion was established when the portion of the fault used was equivalent to four station distances. This implies that such calculations depend strongly on location of the observation point. Even though a simplification can be expec expected with a careful choice of fault segment, there seems to be no simple formula for this procedure.

REFERENCES

1. Mal, A.K., "Applications of Continuum Mechanics," Applied Mechanics Symposia Series of the ASME, No. AMD 8, 1974, pp. 205-223.

2. Richards, P.G., "Dynamic Motions Near an Earthquake Fault: A Three Dimensional Solution," Bull. Seism. Soc. Am., Vol. 66, 1976, pp. 1-32.

3. Levy, N.A. and A.K. Mal, "Calculation of Ground Motion in a Three-Dimentional Model of the 1966 Parkfield Earthquake," Bull. Seism. Soc. Am., Vol. 66, 1976, pp. 405-423.

ACKNOWLEDGMENT

This research was supported by the National Science Foundation (RANN) under Grant GI 44076.

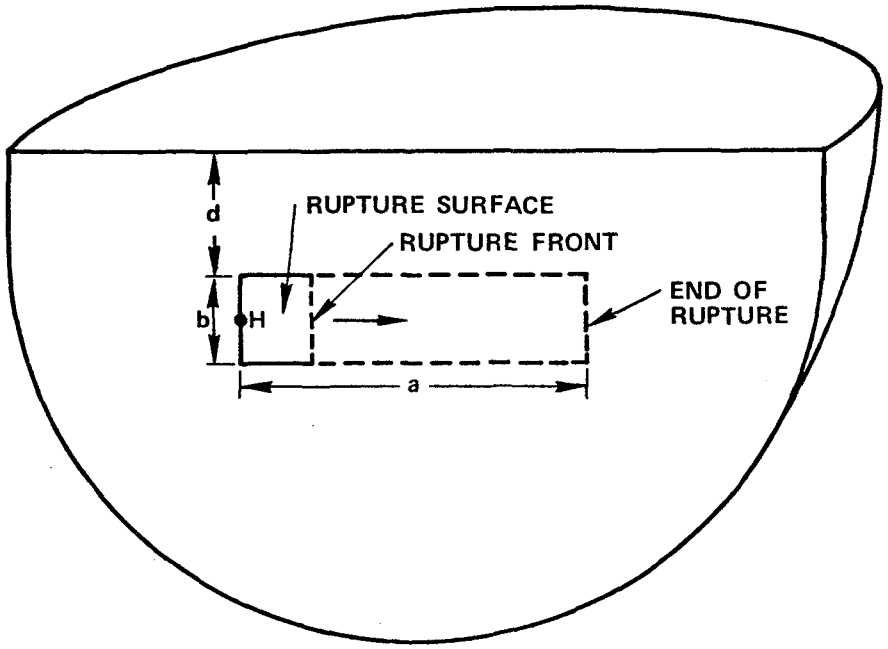

Figure 1. The Geometry of the Problem.

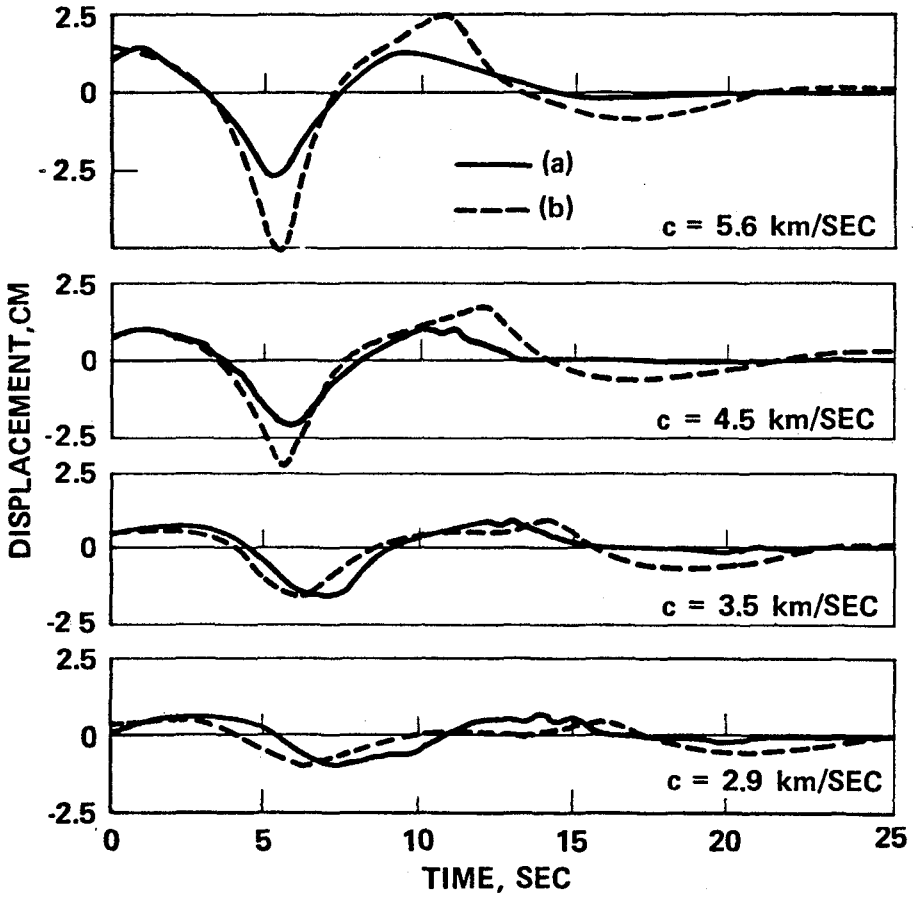

Figure 2. Horizontal Displacement Components Normal to Fault Plane: (a) Strike-slip Faulting. (b) Dip-slip Faulting.

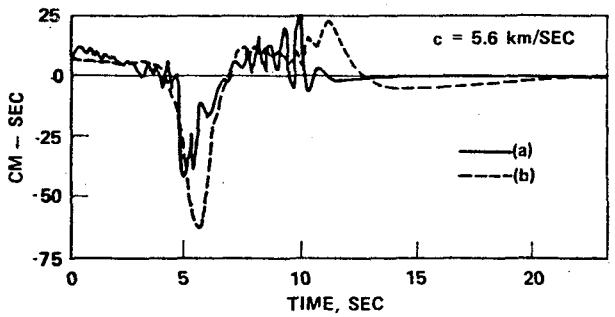

Figure 3. Same as in Figure 2 for Velocities.

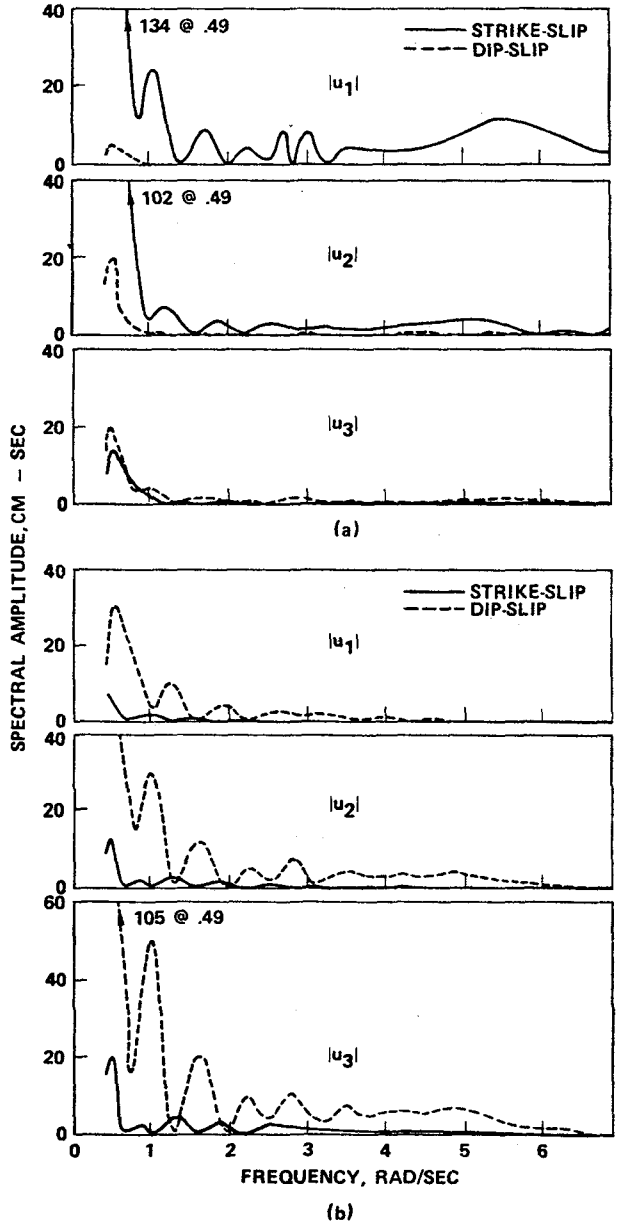

Figure 4. Displacement Spectra for Strike and Dip-slips: (a) Body Waves, (b) Rayleigh Waves.

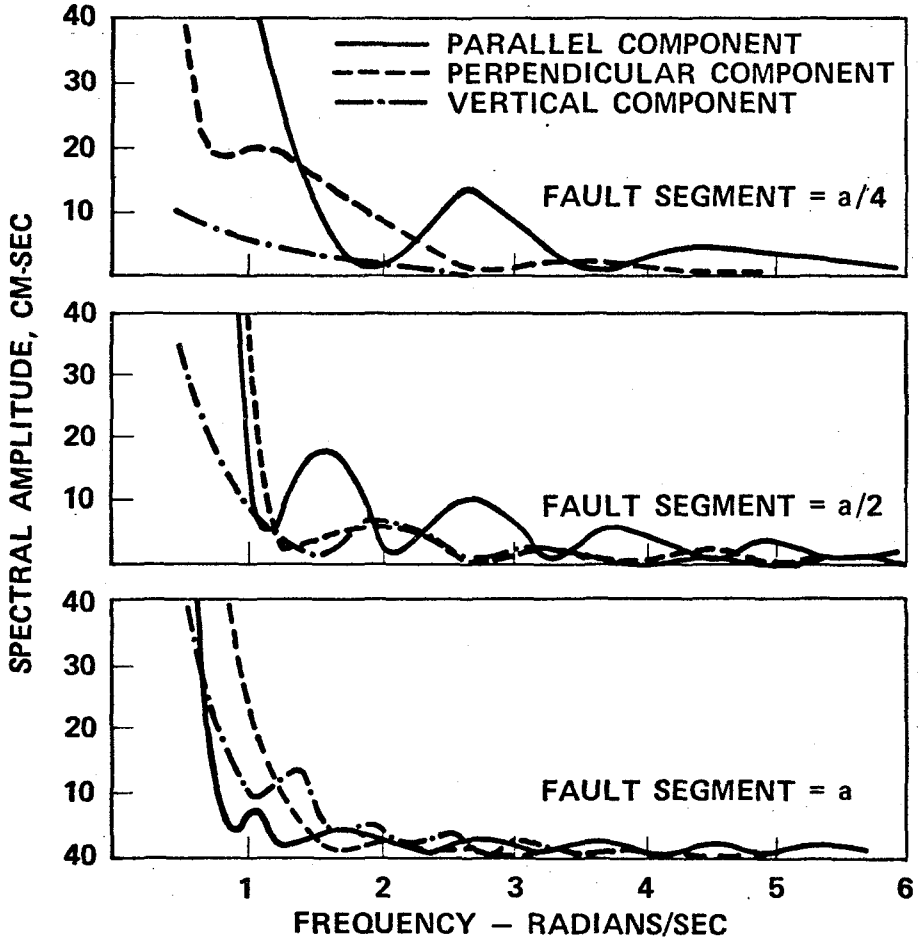

Figure 5. Displacement Spectra for Strike-Slip Faulting Calculated from Fault Segments.

SEPARATION OF BODY AND SURFACE WAVES IN STRONG GROUND MOTION RECORDS

George C. Liang[I] and C. Martin Duke[II]

SYNOPSIS

A method[1] to separate body and surface waves in strong motion accelerograms is presented. This method incorporates a linear system model which accounts for the behavior of both body and surface waves. To demonstrate the method, Fourier spectra of the mainshock records from the 1971 San Fernando earthquake are used. Spurious peaks occurred in many calculations due to divisions of Fourier spectra. A multi-station scheme which eliminates the spurious peak problem is presented.

INTRODUCTION

A number of strong motion accelerograms were collected from the 1971 San Fernando earthquake. These records were digitized and corrected for errors by the California Institute of Technology. Among these records, three mainshock accelerograms at ground levels, that is 8244 Orion Avenue, 15250 Ventura Blvd. and 1800 Century Park East, are used in this presentation. Fig. 1 illustrates the relative locations of these stations with respect to the epicenter.

SYSTEM MODEL

In order to understand fully the behavior of the ground during an earthquake, it is desirable to incorporate the source, the transmission path, and the local site geology simultaneously in the analysis. An approach may be made using linear system theory. This theory manipulates the accelerograms in the frequency domain by making use of the concept on transfer function[2]. A simple linear system model[3] which incorporates the characteristics of both body and surface wave is shown in Fig. 2. The symbols E, R, W, X, and G represent respectively the source functions, the radiation patterns, the path transfer functions, the local site characteristics, and the ground motions; with the subscript b denoting body wave and s denoting surface wave. All the functions are in frequency domain. These functions are related by the following two linear equations.

$$G_s = E_s R_s W_s X_s$$
$$G_b = E_b R_b W_b X_b \qquad (1)$$

The computation of the radiation patterns R_b and R_s are obtained[1] using a model of a double couple source in a semi-infinite medium. The path transfer functions W_b and W_s are modeled using damped spherical

---

I Postgraduate Research Engineer, School of Engineering and Applied Science, University of California, Los Angeles, California.

II Professor of Engineering, University of California, Los Angeles, California.

equations for body waves and damped cylindrical spreading equations for surface waves.[1,2] The modeling of the local site characteristics for the body waves, X_b is based on the Haskell-Thomson method[4] with SH-waves propagating vertically through horizontal layers. Actual soil profiles for the sites[5] are used for the modeling. The local site characteristics for surface waves, X_s, is not so well defined as yet. It is assigned unit amplitude for all frequencies in this analysis.

METHOD OF SEPARATION

The method for separating body and surface waves makes use of two stations and one earthquake event. Based on the system model presented in Eq. (1) and Fig. 2, the following set of linear equations can be written.

$$\begin{aligned} G_{s1} + G_{b1} &= G_1 \\ G_{s2} + G_{b2} &= G_2 \\ G_{s1} \,/\, G_{s2} &= M \\ G_{b1} \,/\, G_{b2} &= N \end{aligned} \tag{2}$$

where G_{s1}, G_{s2} and G_{b2} are the body and surface wave components at stations 1 and 2. These are the unknowns in the above set of linear equations. G_1 and G_2 are the Fourier transforms of the actual accelerograms recorded at the two sites, and M and N are known quantities which can be calculated from the equations shown below.

$$\begin{aligned} M &= \frac{R_{s1}\, W_{s1}\, X_{s1}}{R_{s2}\, W_{s2}\, X_{s2}} \\ N &= \frac{R_{b1}\, W_{b1}\, X_{b1}}{R_{b2}\, W_{b2}\, X_{b2}} \end{aligned} \tag{3}$$

A set of equations for calculating the body and surface wave contents for the two stations can be obtained by solving the set of linear equations in Eq. (2). These equations are shown below.

$$\begin{aligned} G_{s2} &= \frac{NG_2 - G_1}{N - M} \quad ; \qquad G_{s1} = \frac{M(NG_2 - G_1)}{N - M} \\ G_{b2} &= \frac{G_1 - MG_2}{N - M} \qquad\quad G_{b1} = \frac{N(G_1 - MG_2)}{N - M} \end{aligned} \tag{4}$$

where all the variables are functions of frequency.

Two sets of calculated body and surface wave spectra for station Orion are presented in Fig. 3 and 4. The station pairs used for the computations are Orion and Ventura; and Orion and Century Park East. Fig. 5 shows the psectrum for the recorded ground motion at Orion.

SPURIOUS PEAKS

The separated body and surface wave spectra shown in Fig. 3 and 4 are not quite satisfactory due to the presence of spurious peaks. This is especially pronounced in Fig. 4. These spurious peaks tend to dominate the records, thus yielding undesirable inverse transform time histories.[1]

A multi-station procedure is used for eliminating these spurious peaks. By making use of the separated body and surface wave spectra at the same station obtained from two independent sets of calculations, an acceptable set of separated body and surface wave spectra can be obtained. This is done by combining these sets of independently calculated spectra for the same components using different weighing factors. Fig. 6 shows the combined results for station Orion. Note that the spurious peaks are reduced quite significantly.

RESULTS

This presentation provides a method to separate body and surface wave contents in strong motion accelerograms. The method requires Fourier transforms of the accelerograms at two stations. In addition, the complete transfer functions from the source to the site for both stations are also needed. Two sets of separated spectra for the body and surface wave contents are presented. A method for eliminating spurious peaks from the calculations is also examined. However, all these calculations provide only a preliminary evaluation on the separation technique. The reliability of these calculations is yet quite rough. In order to achieve better reliability, the modeling of the transfer functions ought to be improved so that all the important influences on the seismic waves can be incorporated. Also, a better method for avoiding spurious peaks is needed.

ACKNOWLEDGMENT

The authors' thanks are extended for assistance by Professors Ajit K. Mal and Lawrence K. McNamee of the University of California, Los Angeles, Jeffrey A. Johnson of Dames and Moore, Peter J. Hradilek of the U. S. Army Corps of Engineers, and Kenneth W. Campbell of Leroy Crandall and Associates. Financial support was provided by the National Science Foundation (GI44056) and is gratefully acknowledged.

REFERENCES

1. Liang, G. C. "Separation of Body and Surface Waves in Strong Ground Motion Records," Master of Science Thesis, University of California, Los Angeles, UCLA-ENG-7627, March 1976.

2. Duke, C. M. and A. K. Mal. "A Model for Analysis of Body and Surface Waves in Strong Ground Motion," Proc. U. S. Nat'l. Conf. on Earthquake Engr., EERI, pp. 17-24, 1975.

3. Duke, C. M. and P. J. Hradilek. "Spectral Analysis of Site Effects in the San Fernando Earthquake," Proc. of the Fifth World Conf. on Earthquake Engr., Rome, Italy, 1973, Vol. 1, Session 26, No. 77, Ministry of Public Words, Rome, Italy, 1973.

4. Haskell, N. A. "The Dispersion of Surface Waves in Multilayered Media," Bull. Seis. Soc. Am., Vol. 65, pp. 4147-4150, 1960.

5. Duke, C. M., J. A. Johnson, Y. Kharraz, K. W. Campbell and N. A. Malpiede. "Subsurface Site Conditions and Geology in the San Fernando Earthquake Area," School of Engineering and Applied Science, University of California, Los Angeles, UCLA-ENG-7206, December 1971.

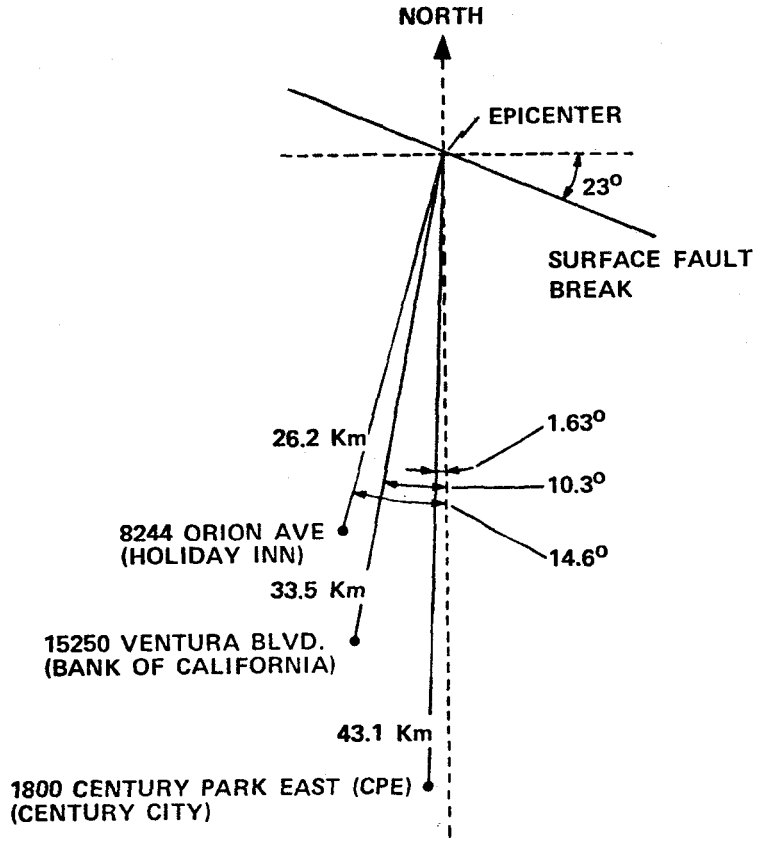

Figure 1. Stations Used in the Analyses.

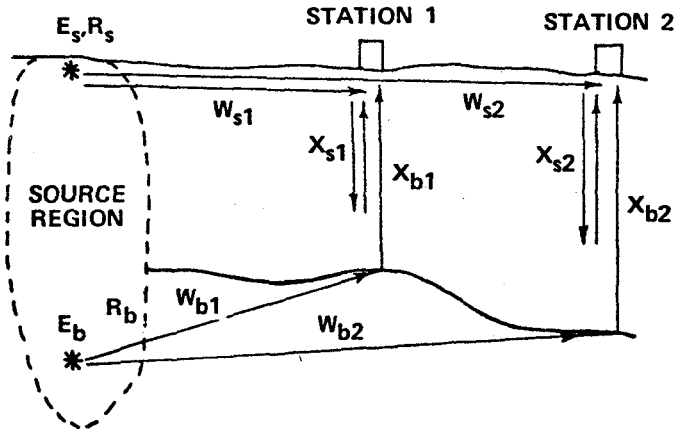

Figure 2. Linear System with Two Stations.

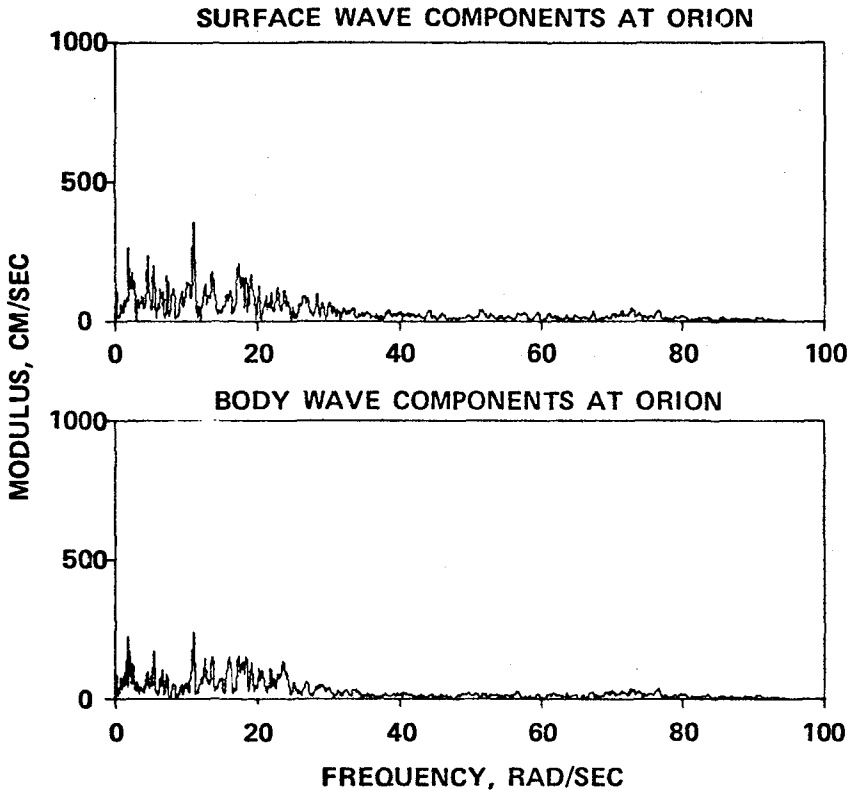

Figure 3. The Separated Spectra for Orion, Orion and CPE Pair.

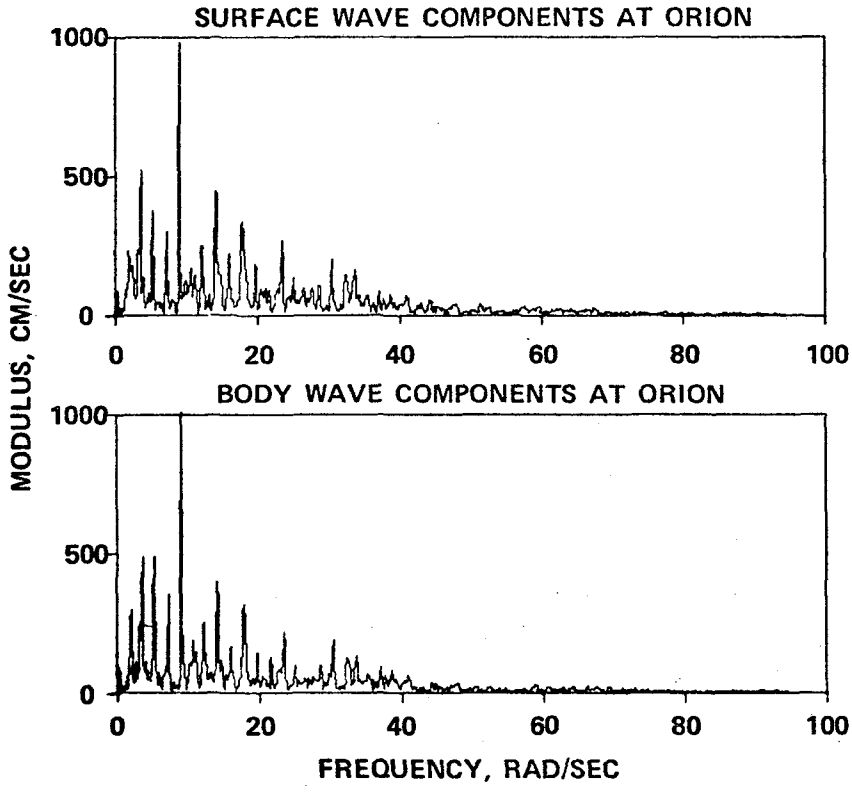

Figure 4. The Separated Spectra for Orion, Orion and Ventura Pair.

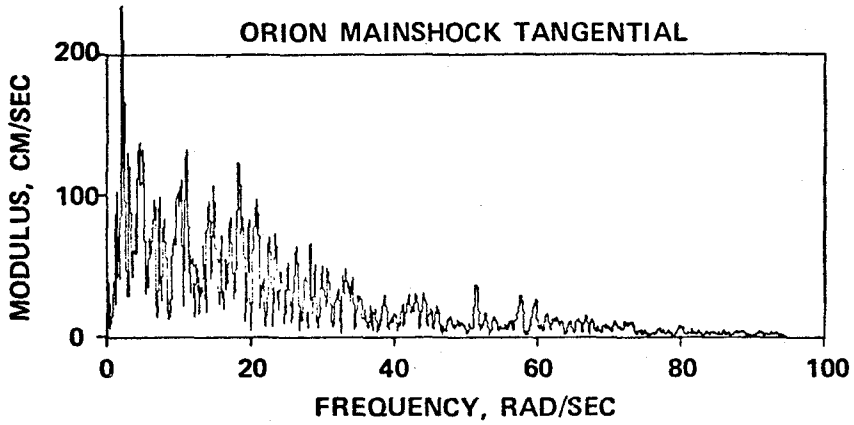

Figure 5. Spectrum of Recorded Ground Motion at 8244 Orion.

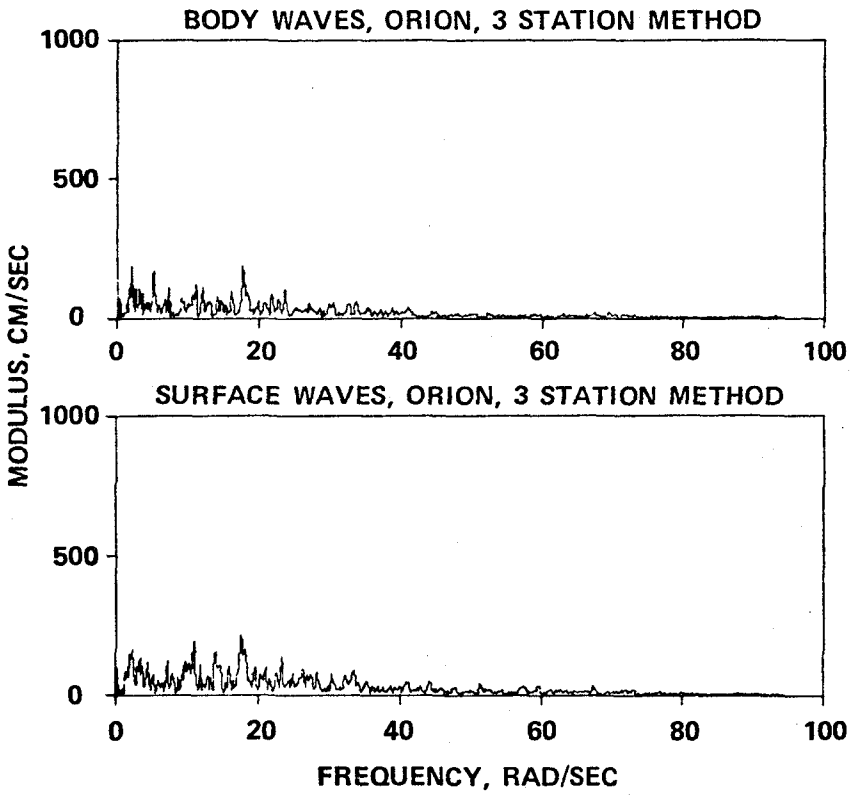

Figure 6. Combined Spectra for Body and Surface Waves at 8244 Orion.

TRANSFER FUNCTIONS FOR SURFACE WAVES

by

A.K. Mal[I] and C.M. Duke[I]

SYNOPSIS

An approximate technique is developed to calculate the surface wave transfer functions for propagation between two stations with different site conditions. The technique is applied to Love waves propagating in a two dimensional single-layered model of the soil containing a discontinuous change in the layer thickness. The displacement spectra produced by sudden dislocation near the free surface at two stations located on either side of the transitional zone are calculated and compared. The influence of the higher modes is shown to be highly significant, especially at higher frequencies.

INTRODUCTION

In most of the previous studies on the influence of local site conditions on earthquake ground motion it has been implicitly assumed that no significant seismic energy is propagated along the sedimentary layers and that the motion produced within the underlying bedrock can be adequately described by means of body waves with appropriate decay factors. It is difficult to justify the validity of these assumptions in shallow earthquakes where a significant amount of energy is trapped in the layers as surface waves. In order to improve the applicability of such studies the present authors are in the process of developing a linear system model which incorporates the transfer functions of both body and surface waves [1].

In an attempt to give a proper definition of the surface wave transfer functions and to understand the mechanics of energy transfer across transitional regions we consider a single layered model of the earth containing a sudden change in layer thickness caused by a step change in the elevation of the interface. We study the propagation of Love waves in the model, with special emphasis at high frequencies. The technique can be extended to multilayered media and Rayleigh waves.

In almost all of the previous studies on the propagation of surface waves in layers of varying thickness the influence of the higher modes have essentially been ignored. Since the higher modes become highly significant at high frequencies, the results of such studies cannot be directly used in earthquake engineering applications. We describe an alternate approximate technique which is more accurate at higher frequencies.

THEORY

Let H_1 and H_2 denote the layer thicknesses to the left and the right of the discontinuity. μ_1, β_1 are the shear modulus and the shear wave velocity of the layer while μ_2, β_2 are those for the basement complex. We introduce a

[I]Professor, Department of Mechanics and Structures, University of California, Los Angeles, California 90024.

cartesian system (x,y) at the surface on the left side of the step at a distance d from it. The x axis is horizontal, to the right and y-axis vertically downward.

At a given frequency ω let N_1, N_2 denote the number of Love modes that can exist in the layers of thickness H_1 and H_2 respectively. Then an incident Love wave with mode number ℓ, surface amplitude one and frequency ω will give rise to N_1 reflected modes and N_2 transmitted modes at the step. Let $A_{\ell m}$, $B_{\ell n}$ denote the surface amplitudes of the m^{th} reflected mode and the n^{th} transmitted mode. Then the spectral surface displacements to the left and the right of the discontinuity may be expressed in the form,

$$u_\ell(x,0,\omega) = e^{ik_\ell x} + \sum_{m=1}^{N_1} A_{\ell m} e^{ik_\ell d - ik_m(x-d)}, \quad 0 < x < d, \tag{1a}$$

$$= \sum_{n=1}^{N_2} B_{\ell n}\, e^{ik_\ell d + ik_n(x-d)}, \quad x > d, \tag{1b}$$

where k_ℓ, k_m, k_n denote the wave numbers of the incident, reflected and the transmitted modes and the phase shift of each wave has been taken into account. The second expression (1b) in the right hand side gives the amplitude and phase of the transmitted Love wave and will be called the modal transfer function for the ℓ^{th} mode. It is to be noted that although the incident wave amplitude is a constant (unity) the transmitted and reflected waves have amplitudes which vary with x.

The coefficients $A_{\ell m}$, $B_{\ell n}$ cannot be calculated exactly. It can be shown, by using the orthogonality properties of the Love modes and the continuity of the displacement across $x = 0$, that,

$$A_{\ell m} = \int_0^\infty \mu(y,H_1)\, U_m(y,H_1) \left\{V_\ell(y) - U_\ell(y,H_1)\right\} dy \Big/ R_m(H_1)$$

$$B_{\ell n} = \int_0^\infty \mu(y,H_2)\, U_n(y,H_2)\, V_\ell(y)\, dy \Big/ R_n(H_2) \tag{2}$$

where

$$R_m(H) = \int_0^\infty \mu(y,H)\,[U_m(y,H)]^2\, dy$$

$$\mu(y,H) = \mu_1, \quad 0 < y < H$$

$$= \mu_2, \quad y > H$$

$U_m(y,H)$ is the Love wave mode shape in the m^{th} mode defined in [2] and $V_\ell(y)$ is the (unknown) displacement along the line $x = 0$, $y > 0$. We calculated $V_\ell(y)$ approximately by utilizing a technique similar to that used in [3]. The details are omitted. We only note that the accuracy of the approximation increases with increasing frequency.

We now introduce a sudden strike slip dislocation of magnitude D on a small fault segment $\delta\ell$, oriented at angle θ with the horizontal located at (0,h) in the layer. Then the Love wave spectral displacement produced at a site (x,0) is given by

$$u(x,0,\omega) = \sum_{\ell=1}^{N_1} A_\ell u_\ell(x,0,\omega) \tag{3}$$

where u_ℓ is given in equation (1) and A_ℓ can be found in [2].

NUMERICAL RESULTS

The computations are carried out for the case, $\beta_1 = 1$ km/sec., $\beta_2 = 1.8$ km/sec., $\mu_2/\mu_1 = 3.3$, $H_1 = 1$ km., $H_2 = 1.3$ km or, $H_1 = 1.3$ km, $H_2 = 1$ km.

In Fig. 1 the amplitudes of the modal transfer functions given by (1b) are plotted for the case x = d. Each curve in Figs. (1a) and (1b) represents the amplification of the ℓ^{th} mode Love wave just after it crosses the discontinuity. The amplitude of a given mode approaches unity at very high frequencies. It is to be noted however that at any given frequency at least one mode is strongly affected by the step. The waves propagating from the thick end of the layer are more severely affected by the transition than those propagating from the thin side.

The spectral amplitudes of the Love waves produced at two sites located on either side of the step at a distance of 1 km from it are plotted in Figs. 2 and 3. The source parameters used in these computations are, d = 8 km, h = .25 km, and $\theta = 45°$. Only the incident waves are plotted for the site located to the left of the discontinuity since the reflection coefficients $A_{\ell m}$ have a relatively insignificant effect on the motion. It can be seen that in either case the spectral amplitudes at the two sites differ considerably especially at high frequencies. These difference cannot be related to the contrast in the site properties in a simple manner. They are caused mainly by the transmission of and subsequent interference between the higher modes.

REFERENCES

1. Duke, C.M. and A.K. Mal, "A Model for Analysis of Body and Surface Waves in Strong Ground Motion," Proc. U.S. Natl. Conf. in Earthq. Engr., U. of Michigan, 1975.

2. Nemani, D. and A.K. Mal, "Short Period Surface Waves in a Layered Medium," These Proceedings.

3. Knopoff, L. and J.A. Hudson, "Transmission of Love waves past a Continental Margin," J. Geophys. Res., Vol. 69, 1964, pp. 1649-1653.

ACKNOWLEDGMENT

This research was supported by the National Science Foundation (RANN) under grant GI 44076.

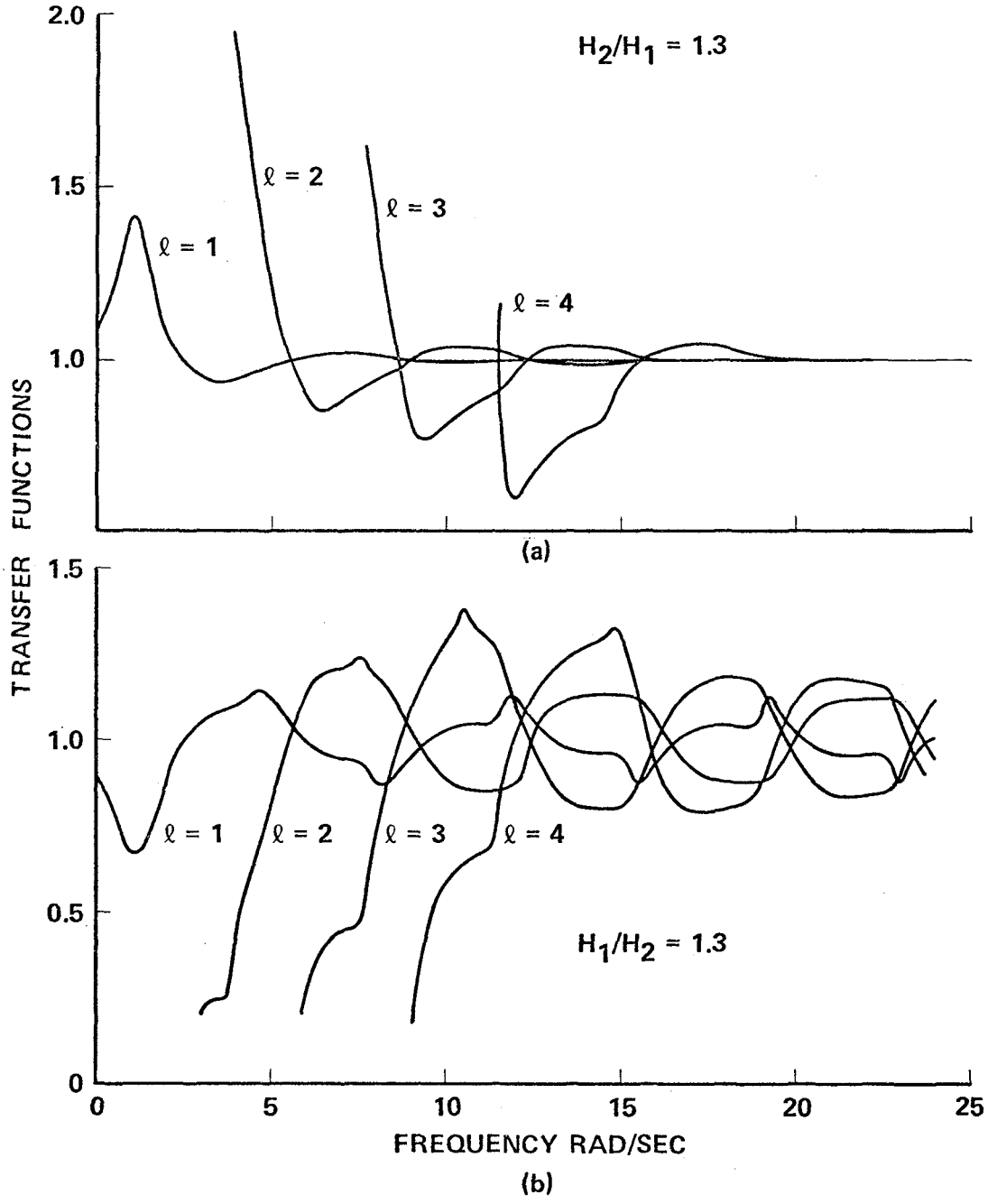

Figure 1. Modal Transfer Functions for Love Waves. ℓ is the Incident Mode Number.

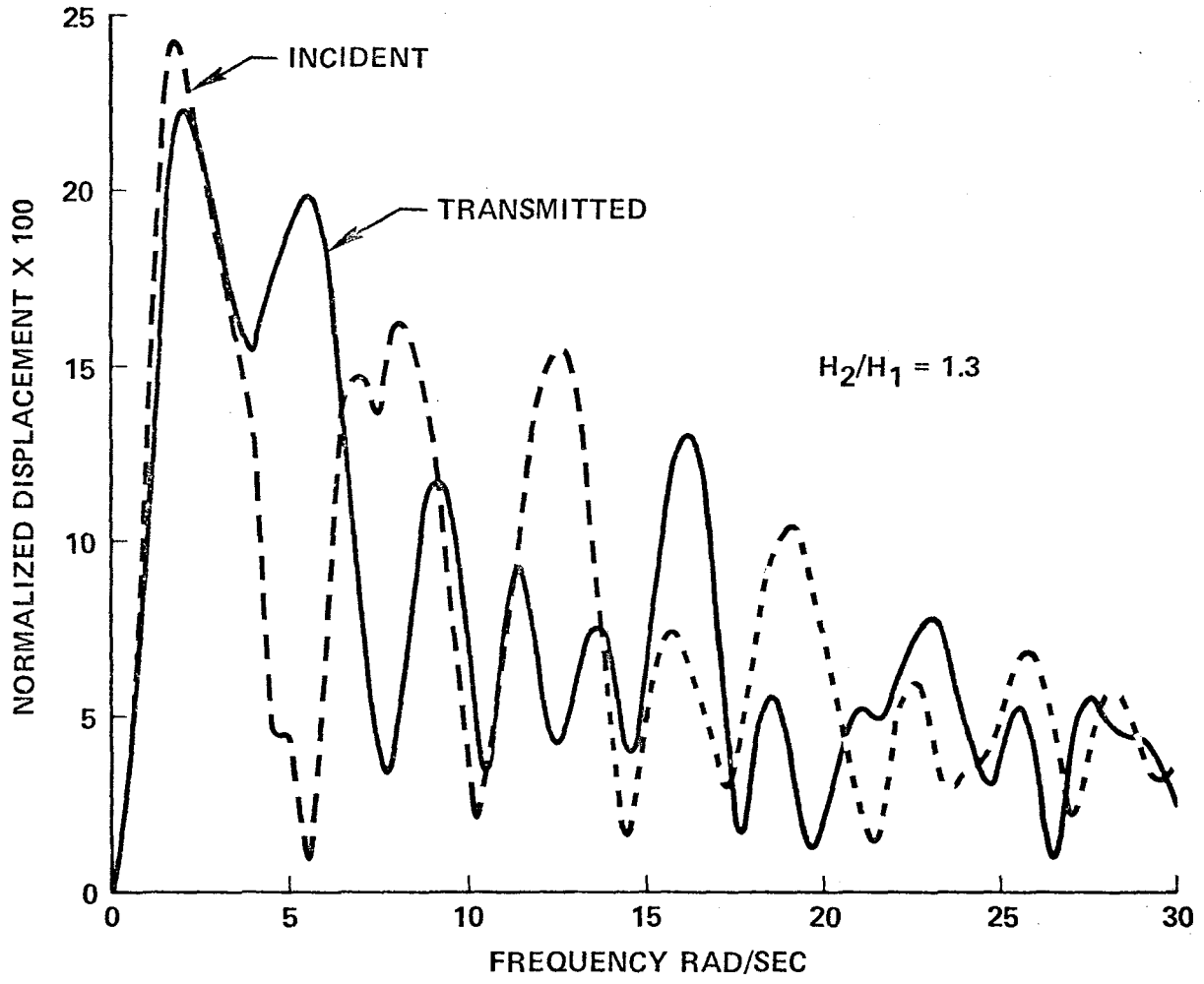

Figure 2. Normalized Love Wave Spectra $|\beta_1 u/D\delta\ell|$ Due to a Near-Surface Point Dislocation at Sites on Either Side of the Discontinuity.

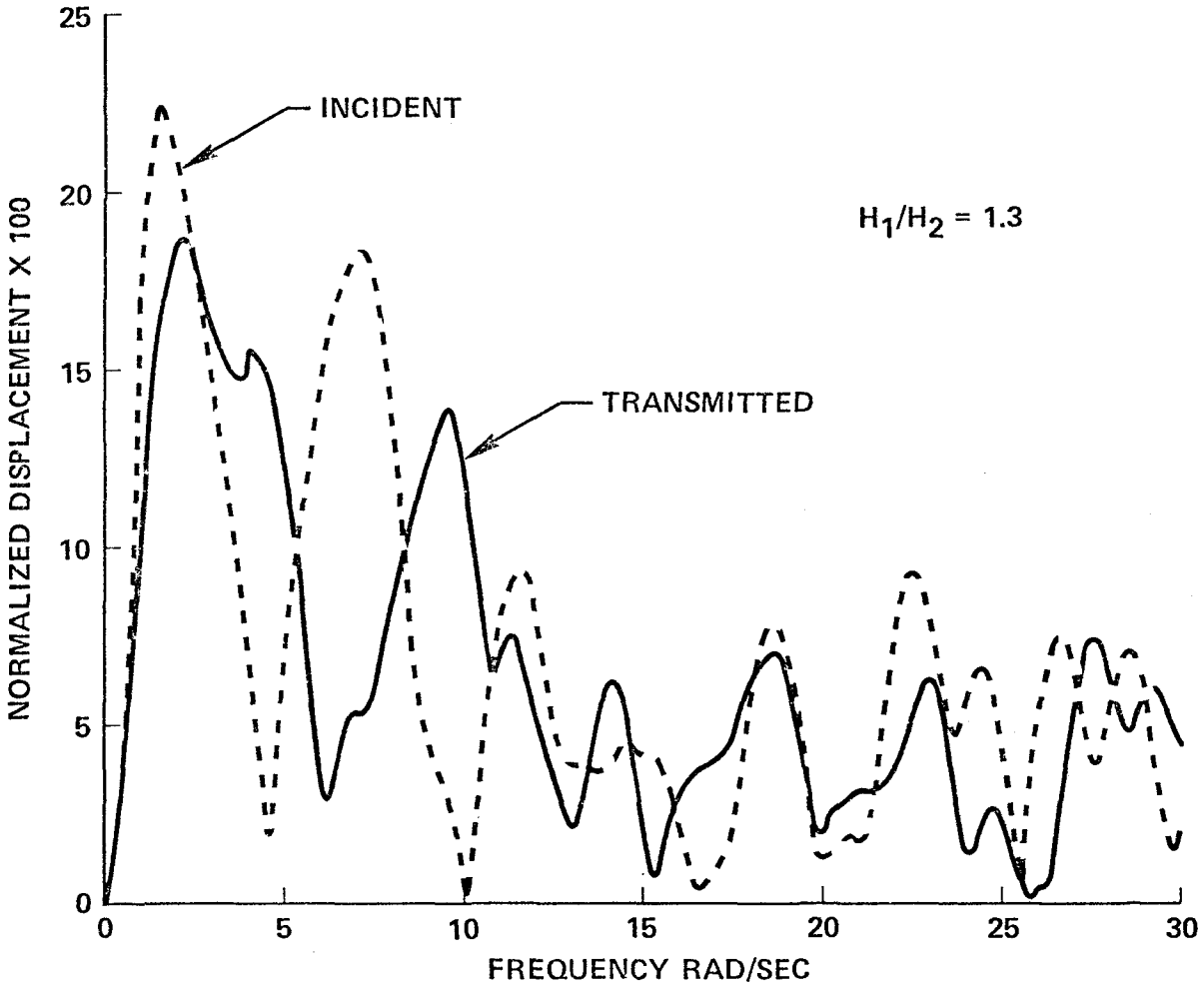

Figure 3. Normalized Love Wave Spectra $|\beta_1 u/D\delta\ell|$ Due to a Near-Surface Point Dislocation at Sites on Either Side of the Discontinuity.

SHORT PERIOD SURFACE WAVES IN A LAYERED MEDIUM

by

D. Nemani[I] and A.K. Mal[II]

SYNOPSIS

In this paper we investigate some properties of surfaces waves at relatively short periods and small epicentral distances by means of existing seismological techniques. We assume a single layered model of the earth and calculate the Love wave displacement spectra that would be produced by shallow earthquake sources located within the layer. The interference between the higher modes is shown to be a significant factor in producing complex ground motions. The amplification of the waves between the interface and the free surface is shown to have a highly anomalous behavior due to the presence of the higher modes.

INTRODUCTION

A majority of the studies on site effects have so far been carried out under the assumption that all of the energy released by the source travel as spherical body waves through bedrock and propagate vertically thereafter as plane waves through the layers. While this may be approximately true for deep focus earthquakes, there is strong evidence that in shallow earthquakes a large percentage of the energy is trapped in the layer and propagate horizontally as surface waves. The amplitudes of the surface waves decay less rapidly than those of body waves with epicentral distance and frequency.

Thus it appears that in strong ground motion studies the contribution of the surface waves must be carefully assessed. Although a large body of seismological literature exists on the subject, most of the available results are applicable at long periods (> 10 sec.) and large epicentral distances (> 100 km). We are currently involved in a systematic study of surface waves at shorter periods (.1-10 sec.) and smaller epicentral distances (10-100 km). In this note we present a number of results based on our preliminary investigation of Love waves propagating in a single layered two dimensional medium.

THEORY

The theory of Love wave propagation is well established and can be found in standard seismological literature (see, e.g. [1]). We quote only the relevant results.

The Love wave phase velocity c_n in a single layered medium of layer thickness H is the real root of the equation,

$$\eta_{1n}H = n\pi + \tan^{-1}(\mu_2\eta_{2n}/\mu_1\eta_{1n}),\ n = 0,1,2,... \qquad (1)$$

[I] Graduate Student

[II] Professor, Department of Mechanics and Structures, University of California at Los Angeles.

where n is the mode number,

$$\eta_{1n} = \omega(\beta_1^{-2}-c_n^{-2})^{1/2}, \quad \eta_{2n} = \omega(c_n^{-2}-\beta_2^{-2})^{1/2},$$

ω is the circular frequency, μ_1, β_1 are the shear modulus and the shear wave velocity in the layer and μ_2, β_2 are those in the half space. It can be shown that $\beta_1 \leq c_n \leq \beta_2$ and that the higher modes appear at the cut off frequencies,

$$\omega = \omega_n = n\pi\beta_2/H\{(\beta_2/\beta_1)^2-1\}^{\frac{1}{2}}, \quad n = 1,2,... \tag{2}$$

Taking the x-axis along the horizontal and y-axis vertically downward from the free surface, the displacement spectrum at any point within the layer may be expressed in the form,

$$u(x,y,\omega) = \sum_{n=0}^{N(\omega)} U_n(y,\omega)\exp(i\omega x/c_n) \tag{3}$$

where $N(\omega)$ is the number of modes present at frequency ω, and the mode-shape functions $U_n(y,\omega)$ with surface amplitude S_n are given by

$$U_n(y,\omega) = S_n\cos(\eta_{1n}y), \quad 0 \leq y \leq H$$

$$= S_n\cos(\eta_{1n}H)\ \exp\{-\eta_{2n}(y-H)\}, \quad y \geq H \tag{4}$$

In order to calculate S_n we introduce a strike-slip dislocation of (small) length $\delta\ell$ and dip angle θ located at depth $h(< H)$ on the y axis. We assume that the dislocation has a time dependence $f(t)$ so that the source (displacement) spectrum is $F(\omega)$, the Fourier transform of $f(t)$. It can be shown that for $x > 0$,

$$S_n = 2\delta\ell F(\omega)\ (P_n\sin\theta + i\ Q_n\cos\theta)/R_n \tag{5}$$

where,

$$P_n = \eta_{1n}\cos(\eta_{1n}h), \quad Q_n = \eta_{1n}^2 c_n \sin(\eta_{1n}h)/\omega$$

$$R_n = 2\eta_{1n}H + \{1-(\beta_1/\beta_2)^2\}\ \sin(2\eta_{1n}H)/\{(\beta_1/c_n)^2-(\beta_1/\beta_2)^2\}$$

The amplification of the surface waves between the interface and the free surface can be calculated from (3) through the relation

$$A_s(x,\omega) = |u(x,o,\omega)/u(x,H,\omega)| \tag{6}$$

It may be recalled, for comparison purposes that for plane shear waves with incident angle ϕ the amplification is given by

$$A_B(\omega) = 1/\cos(\nu_1 H) \tag{7}$$

where $\nu_1 = \omega\{\beta_1^{-2}-\beta_2^{-2}\sin^2\phi\}^{1/2}$. Thus resonance occurs at the frequencies,

$$\omega = \Omega_n = (2n+1)\pi\beta_2/2H\{(\beta_1/\beta_2)^2-\sin^2\phi\}^{1/2},\ n = 0,1,2,\ldots \qquad (8)$$

NUMERICAL RESULTS

The numerical results are presented for a model in which $\beta_1 = 1.0$ km/sec., $\beta_2/\beta_1 = 1.3$, $\mu_2/\mu_1 = 3.3$, and $H = 1.3$ km. The solution of (1) for these assumed values of the site parameter is plotted in Fig. 1. It can be seen that the phase velocity is multiple valued for $\omega > 2.2$ rad/sec., and that the number of modes increases to 22 at $\omega = 60$ rad/sec.

In order to calculate the spectral amplitudes we assume that the slip function is a step of magnitude D in time. Then $F(\omega) = iD/\omega$ for $\omega \neq 0$. We further assume that the source is either located near the interface (h = 1 km) or near the free surface (h = .25 km). The normalized spectral surface amplitudes $|u(x,o,\omega)\beta_1/D\delta\ell|$ are plotted against frequency in Fig. 2, for two epicentral distances (x = 8 km, 15 km) in the case of the interface source (h = 1 km). The only common feature in the two curves is the large amplitude near $\omega = 1.2$ rad/sec., which is caused by the fundamental mode alone. The secondary peaks at higher frequencies are more important in earthquake engineering studies. The spectral amplitude at x = 8 km for the surface source (h = .25 km), exhibit more prominent secondary peaks (solid curve, Fig. 2) than that for the interface source (h = 1 km). The complexity of the spectra at high frequencies is caused by strong interference between the higher modes. Although the plots have been terminated at $\omega = 20$ rad/sec. similar pattern is repeated at higher frequencies.

In order to further examine the influence of the site parameters on the surface motion the amplification factors $A_s(x,\omega)$ for x = 8 km and 15 km are plotted in Fig. 3 for a source depth of 1 km. The natural frequencies of the layer are also identified in the figure. Comparison of the amplification curves indicates that the surface wave motion at two stations with identical site properties may be considerably different. The peak amplitudes appear to be unrelated to the natural-frequencies of the layer.

We note one additional feature of the spectra. The ω^{-1} decay introduced in the source function is not sufficient to cause significant reductions in the amplitudes at high frequencies. Even with the introduction of damping ($Q \simeq 50$) and geometrical spreading ($\sim (\omega x)^{-1/2}$) factors the velocity and acceleration spectra calculated from the plots in Fig. 3 will have unreasonably large amplitudes at high frequencies. Thus the spectrum of the source function must decay more strongly with frequency, indicating the nexessity of including loss mechanisms at the source.

REFERENCE

1. Ewing, Jardetsky and Press, Elastic Waves in Layered Media, McGraw Hill, 1957.

ACKNOWLEDGMENT

This research was supported by the National Science Foundation (RANN) under grant GI44076.

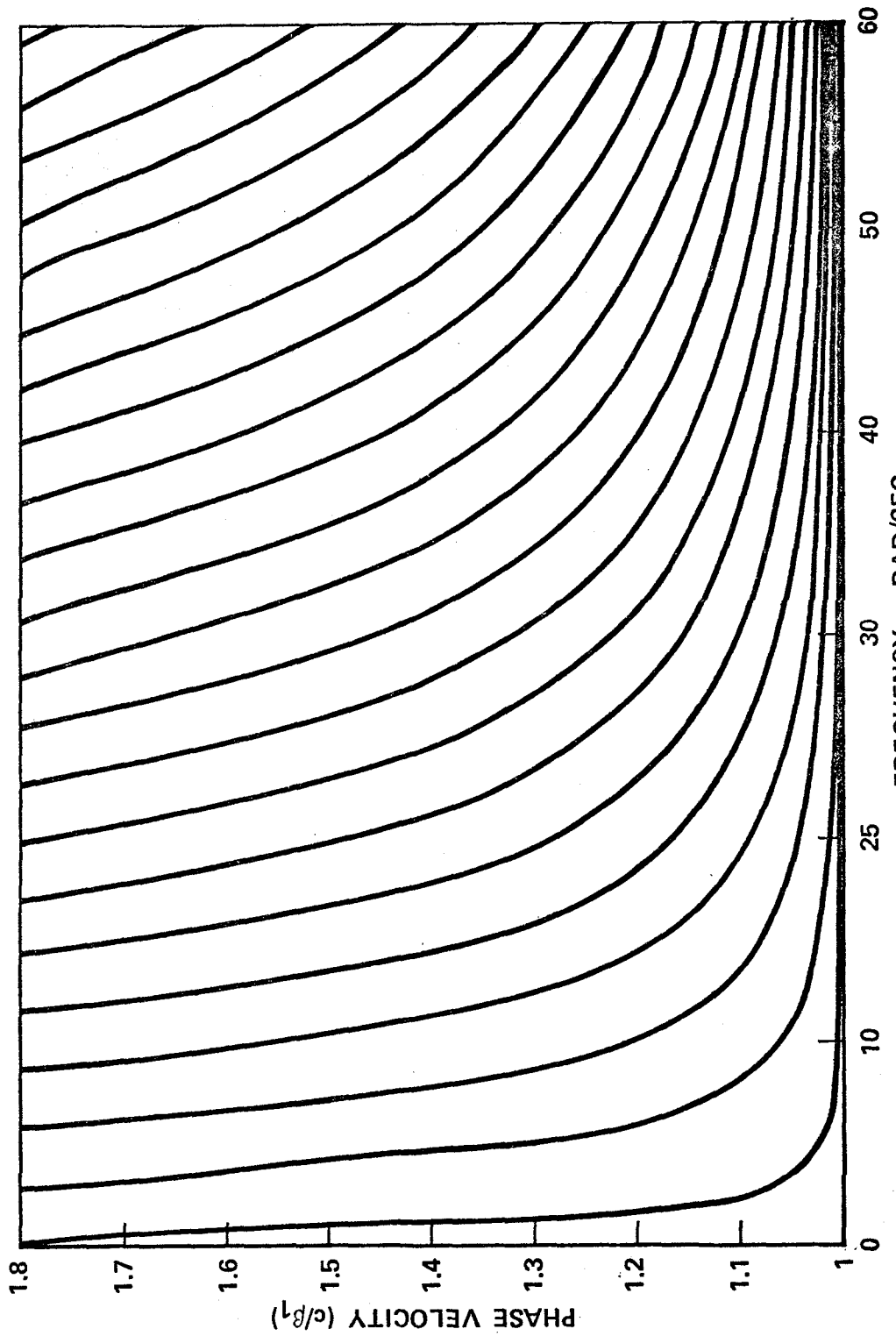

Figure 1. The Love Wave Phase Velocity Curves.

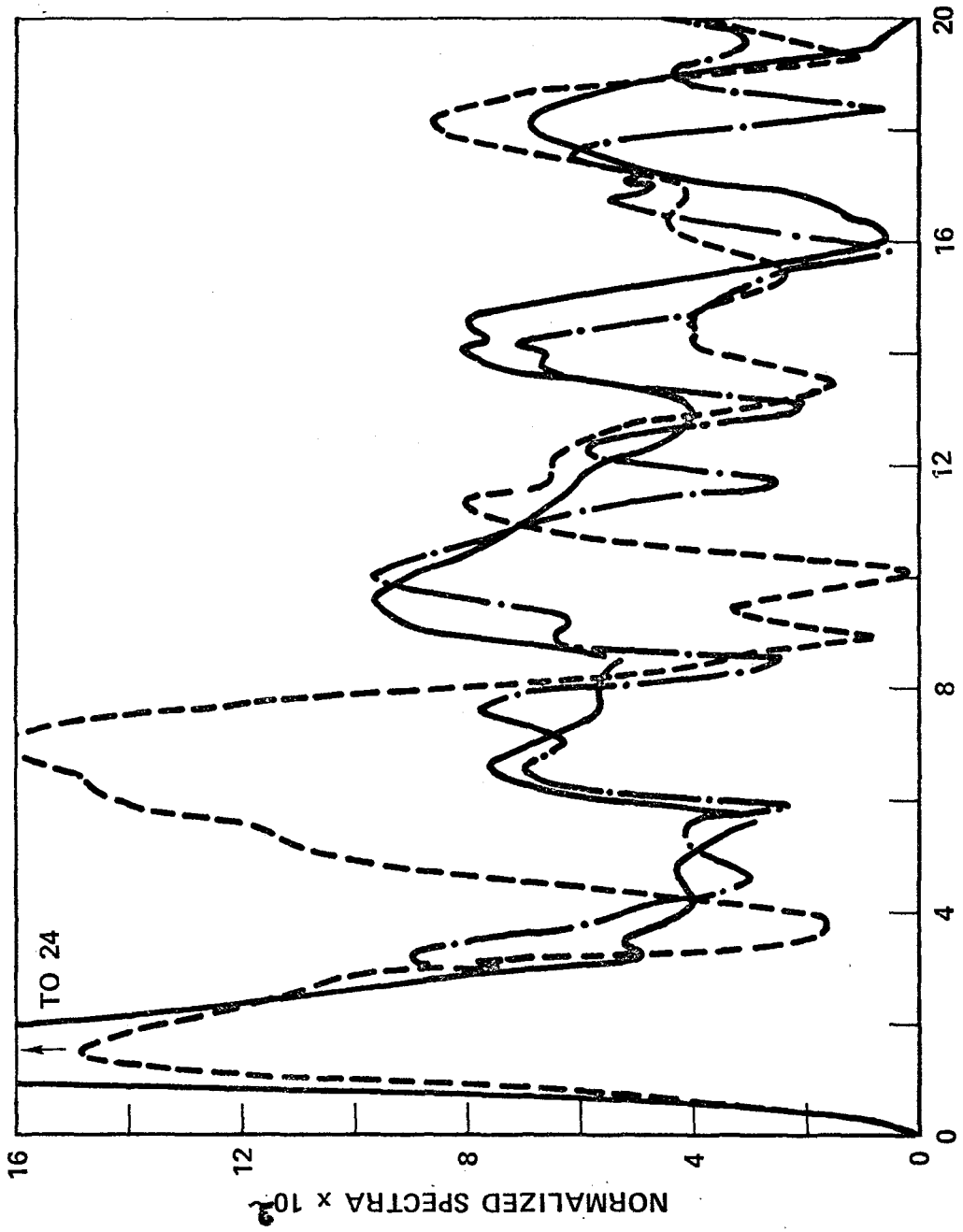

Figure 2. Normalized Displacements ; $|\beta_1 u(x,o,\omega)/D\delta\ell|$.
Solid — h = 1 Km, x = 8 Km, Dash–dots— h = 1 Km., x = 15 Km,
Dashes — h = .25 Km, x = 8 Km.

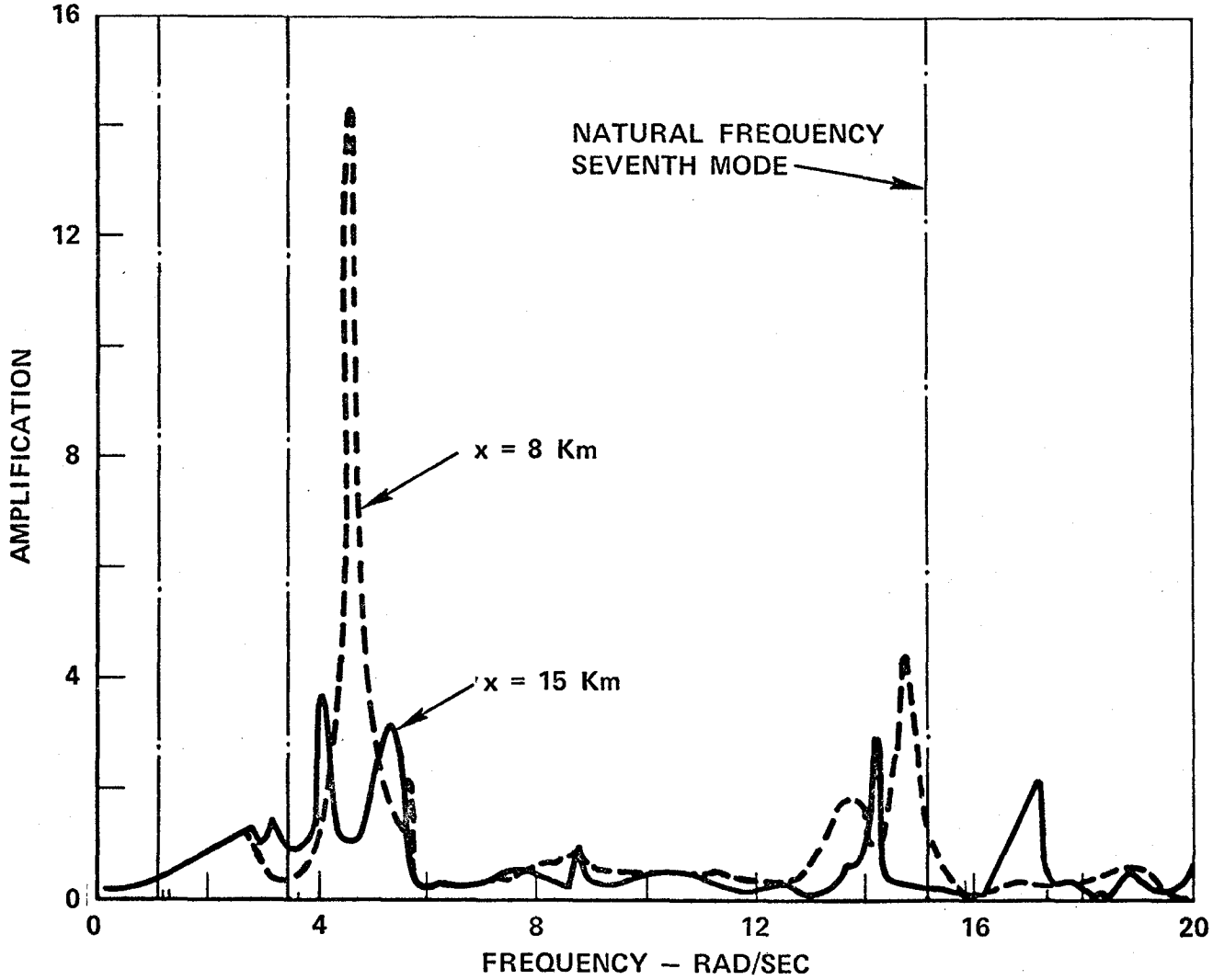

Figure 3. Amplification $|u(x,o,\omega)/u(x,H,\omega)|$ for h = 1 Km. The vertical lines indicate natural frequencies at normal Incidence. *The identified frequencies following these lines are those for incidence angles* of 30^{o} and 60^{o} respectively.

COLLAPSE ANALYSIS OF MULTISTORY BUILDINGS

by

Lawrence G. Selna[I]

INTRODUCTION

After a building is noticeably damaged in an earthquake, the earthquake engineer needs to know if the building should be repaired. A method of static incremental analysis suitable for predicting the likelihood of collapse is needed.

The objectives of this paper are to: 1) develop a method for large deflection quasi-static incremental analysis of ductile reinforced concrete frames, and 2) interpret the results of static collapse studies. The frames studied are loaded incrementally with static loads simulating earthquake-like load distributions.

ANALYSIS PROCEDURE

Quasi-static incremental displacement analysis which considers the decrease in story shear resistance after yield can be formulated either with the incremental displacements or incremental forces as the dependent variables. Examine the quasi-static equilibrium equation

$$[K_c(u)]_i\{\Delta u\}_i + [K_g(u)]_i\{\Delta u\}_i = \{\Delta f\}_i \tag{1}$$

in which $\{\Delta u\}_i$, $\{\Delta f\}_i$ = incremental displacement, force vectors; $K_c(u)$, $K_g(u)$ = conventional, geometric stiffness matrices dependent on displacement history, u; i = increment number.

Though arbitrarily choosing the incremental force, $\{\Delta f\}_i$, is mathematically sound, in actuality a meaningful collapse displacement history cannot be found this way. The choice of $\{\Delta f\}_i$ becomes exceedingly difficult when the fundamental eigenvalue of $[K_c(u) + K_g(u)]$ becomes negative, as it normally does after a yield mechanism forms in the structure. If the incremental displacements, $\{\Delta u\}_i$, are chosen, then a straightforward multiplication can be used to find the incrementally applied loads. This approach is unsuitable in the present collapse analysis study because the incremental displacement history is unknown in multidegree of freedom systems.

A systematic calculation procedure which avoids guessing $\{\Delta u\}_i$ or $\{\Delta f\}_i$ can be formulated from principles of incremental work. In the procedure the shape of the load vector $\{\Delta f\}_i$ and the incremental work are input quantities. The magnitude of the incremental load and incremental displacements are output from the analysis.

Consider the following load and displacement relationships

$$\{\Delta f\}_i = \Delta\alpha_i \{\Delta \bar{f}\} \tag{2}$$

and $$\{\Delta u\}_i \quad \Delta\alpha_i \{\Delta \bar{u}\}_i \tag{3}$$

I Associate Professor, Mechanics and Structures Department, UCLA

in which $\Delta\alpha_i$ = unknown incremental scalar multiplier; $\{\Delta\bar{f}\}$ = specified constant load shape vector; $\{\Delta\bar{u}\}_i$ = unknown scaled displacement vector. The same unknown scalar, $\Delta\alpha_i$, is used in Eqs. 2 and 3 because $\{\Delta u\}_i$ and $\{\Delta f\}_i$ are linearly related in Eq. 1.

The accumulated load is found from the relation

$$\{f\}_{i+1} = \{f\}_i + \{\Delta f\}_i \tag{4}$$

in which $\{f\}_{i+1}$, $\{f\}_i$ = accumulated loads for increments i+1 and i.

The incremental external work done by the accumulated load, $\{f\}_i$, moving through the incremental displacemtnt $\{\Delta u\}_i$ is given by

$$\Delta W_i = \{f\}_i^T \{\Delta u\}_i \tag{5}$$

in which ΔW_i = incremental external work. In the present paper ΔW_i is a specified quantity whereas in usual equilibrium calculations ΔW_i, is sometimes computed, as an afterthought, from Eq. 5.

An incremental procedure can be devised using Eqs. 1 through 5, but some supportive data must be supplied. Before the incremental procedure is carried out the quantities ΔW_i (i=1, ..., number of increments) and $\{\Delta\bar{f}\}$ must be specified. These are input data whose selection will be discussed in the Section, "Input Quantities." At the beginning of each increment the stiffness matrices $K_c(u)$ and $K_g(u)$ must be known. These matrices may be evaluated using known methods for representing uniaxial (1) and biaxial (2,3) behavior. Also known at the start of the increment is the accumulated load vector $\{f\}_i$.

Then the steps followed in each increment are:

1. Substitute Eqs. 2 and 3 into Eq. 1 to obtain

$$\left[[K_c(u)]_i + [K_g(u)]_i\right]\{\Delta\bar{u}\}_i = \{\Delta\bar{f}\}. \tag{6}$$

   Solve for $\{\Delta\bar{u}\}_i$ using a convenient simultaneous equation solution procedure.

2. Combine Eqs. 3 and 5 to obtain

$$\Delta W_i = \Delta\alpha_i \{f\}_i^T \{\Delta\bar{u}\}_i \tag{7}$$

   ΔW_i is specified, $\{f\}_i$ is known from the previous increment, and $\{\Delta\bar{u}\}_i$ is known from Eq. 6. It follows that Eq. 7 may be modified to solve for the unknown scalar, $\Delta\alpha_i$, i.e.

$$\Delta\alpha_i = \frac{\Delta W_i}{\{f\}_i^T \{\Delta\bar{u}\}_i} \tag{8}$$

3. Using Eqs. 2 and 3 the unknowns $\{\Delta f\}_i$ and $\{\Delta u\}_i$ are computed.
4. The accumulated load for the subsequent increment is found using Eq. 4. In a similar fashion the accumulated displacement can be found from

$$\{u\}_{i+1} = \{u\}_i + \{\Delta u\}_i \tag{9}$$

   in which $\{u\}_{i+1}$, $\{u\}_i$ = accumulated displacement for increments i+1 and i.
5. The $K_c(u)$ and $K_g(u)$ are computed for the subsequent increment. Effects of joint coordinate translation on the K_c and K_u are represented in this step.

INPUT QUANTITIES

Some basic understanding of the generalized force-deflection property of the structure is required for choice of ΔW_i. For the present study on collapse of multistory buildings the total work, W, can be found and the increments of work, ΔW_i, can be selected if the distribution of earthquake loads, seismic coefficients, and maximum drifts are estimated in advance. This is not a restrictive requirement since the validity of the estimation can be tested by evaluating the yield shears and drifts obtained in the analysis. The magnitude of the ΔW_i values can be changed to study convergence for the load, seismic coefficient, and drift estimations.

Consider the generalized force-deflection relation shown in Fig. 1. The generalized force and displacement quantities are computed from the square root of the sum of force components squared. Two incremental work quantities ΔW_3 and ΔW_{30} for increments 3 and 30 are depicted as shaded bar areas. The ΔW_3 is positive for loading while the ΔW_{30} is negative for unloading or reversal. The ΔW_3 has a larger magnitude than ΔW_{30}.

Some properties of the present analysis method are demonstrated in Fig. 1. These properties are: 1) when $[\{f\}_i^T\{f\}_i]^{1/2}$ approaches zero then ΔW_i must be selected to approach zero; otherwise the resulting $[\{\Delta u\}_i^T\{\Delta u\}_i]^{1/2}$ will be a large meaningless quantity; 2) $\Delta W_i > 0$ implies $\{f\}_i^T\{\Delta u\}_i > 0$ and $\Delta W_i < 0$ implies $\{f\}_i^T\{\Delta u\}_i < 0$.

In a collapse analysis of a multistory frame the incremental work is assumed to be positive for all increments. The collapse is signified when the generalized force, $[\{f\}_i^T\{f\}_i]^{1/2}$, approaches zero. The ΔW_i is chosen to approach zero as $[\{f\}_i^T\{f\}_i]^{1/2}$ goes to zero.

APPLICATIONS

Single bay portal frame planar studies are conducted in order to understand the characteristics of the present method. The properties and coordinate idealization of the frame are shown in Fig. 2. The reinforced concrete beam and columns are idealized using the moment-curvature characteristics given in Ref. (1). Each of the elements is divided into three zones. An independent moment-curvature relation is represented in each of the zones.

The vertical loads applied initially but don't enter into the incremental work calculation. The magnitude of the vertical loads has a strong effect on the shear-drift relation (Fig. 3) of the frame. Four axial load levels related to the ideal axial short column capacity, P_o, are used in the study.

The incremental work, ΔW_i, is assumed to be linearly increasing from zero until the story shear reaches a maximum. Then it is assumed to decrease linearly with each increment. The rate of decrease of incremental work per increment is found from the relation

$$\frac{d(\Delta W_i)}{d(i)} = \left[\frac{V_i - V_{imax}}{i - imax}\right] \frac{\Delta W_{imax}}{V_{imax}} \qquad (10)$$

in which $d(\Delta W_i)/d(i)$ = rate of change of incremental work per increment; imax = increment number when story shear is maximum; V_i, V_{imax} = story

shear at increment i, at maximum; ΔW_{imax} = maximum incremental work value. Convergence of shear-drift relations was tested by comparing results of 60 and 120 increment studies. The incremental load shape vector $\{\Delta\bar{f}\}$ is indicated in Fig. 2. The upshot of these assumptions is that $\{\Delta f\}_i$ is positive until the maximum shear is reached. Thereafter it is negative. Meanwhile $\{f\}_i$ and $\{\Delta u\}_i$ are positive for all of the increments.

Several aspects of the shear-drift relations (Fig. 3) are interesting: 1) the initial slope; 2) the maximum value, and 3) the descending slope. The axial load 0.3Po caused maximum initial lateral stiffness and corresponded to the "balanced" axial load. The maximum shear value also occurred for the 0.3Po axial load. The descending slope magnitudes were inversely related to the axial load levels.

The collapse displacements for three axial load levels - 0.3Po, 0.5Po, and 0.8Po - were found to be 0.91 ft, 0.48 ft, and 0.23 ft respectively. The impending collapses were indicated by approach of the generalized force to zero.

In Fig. 4 the critical vertical load is plotted against drift. As with the shear drift relations four axial load levels were used, and three properties of these curves are worthy of discussion.

During the initial stages of loading the frame with column axial loads at balanced condition has the highest critical vertical load. As the lateral load is increased there is a corresponding decrease in the critical vertical load; at this time the critical loads for different vertical load levels merge into a narrow band. When the lateral displacement surpasses yield and the shear-drift relation is descending the critical vertical load is less than the applied vertical load.

Throughout the displacement history the buckling mode shape corresponds to a sway buckling mode.

Multistory planar frame studies are performed to evaluate the adaptability of the present method to large systems. The frame to be studied is shown in Fig. 5. For properties of materials, reinforced concrete element sizes, reinforcement detailing, and structural idealization please refer to Ref. (4).

The incremental load shape vector $\{\Delta\bar{f}\}$ which is intended to represent first mode earthquake loading is assumed to be linearly increasing with height. The vertical load is assumed to come from dead load. The incremental work regime is generated using the same procedure that was used for the portal frame.

Two studies simulating pinned and clamped columns at ground level were performed. The base story shear-drift relation is presented in Fig. 6. For the pinned case the yield mechanism is formed in the first story beams and column pins; in the clamped case yielding occurs at the base of the columns and in the first story beams. The base story shear capacity is approximately three times greater for the clamped case. Collapse displacements were found to be 2.34 ft. for the clamped case and 1.76 ft. for the pinned case.

CONCLUSIONS

The collapse studies performed with the nonlinear incremental work procedure produced a number of interesting results from which the following conclusions are drawn:

1. The shear-drift relation is a curvilinear function starting at zero, going rapidly to a peak, and then declining more gradually back to zero; the shape and magnitude of the relation is influenced by material properties, geometry of the structure, detailing of reinforcement, load configuration, and history.

2. The critical vertical load is a variable quantity. It starts at a high initial value when the undamaged structure is subjected to small lateral loads. The initial value is influenced by the magnitude of the applied vertical load. After yield due to lateral load the critical vertical load is not influenced by the applied vertical load because the lateral loads are dominant.

3. The incremental work procedure can be used to study problems of geometric and material instability. The method is ideally suited for predicting collapse displacements in earthquake damaged structures.

REFERENCES

1. Park, R., Kent, D., and Sampson, R., "Reinforced Concrete Members with Cyclic Loading," J. Struct. Div., ASCE, 98, 1341-1358 (1972).

2. Aktan, A., Pecknold, D., and Sozen, M., "Effects of Two-dimensional Earthquake Motion on a Reinforced Concrete Column," Civ. Engr. Studies, Struct. Res. Ser. Rep., No. 399, Univ. of Ill., Urbana, May 1973.

3. Selna, L. and Lawder, J., "Biaxial Inelastic Frame Seismic Behavior," ACI Symp. Vol., Reinf. Concr. in Seismic Zones (in press).

4. Lee, E.B., "Inelastic Stability Studies of Moment Resistant Frames," UCLA ENGR. M.S. Thesis, 1974.

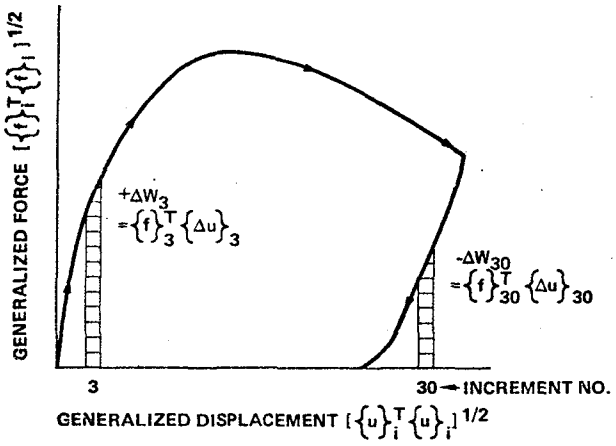

Figure 1. Incremental Work.

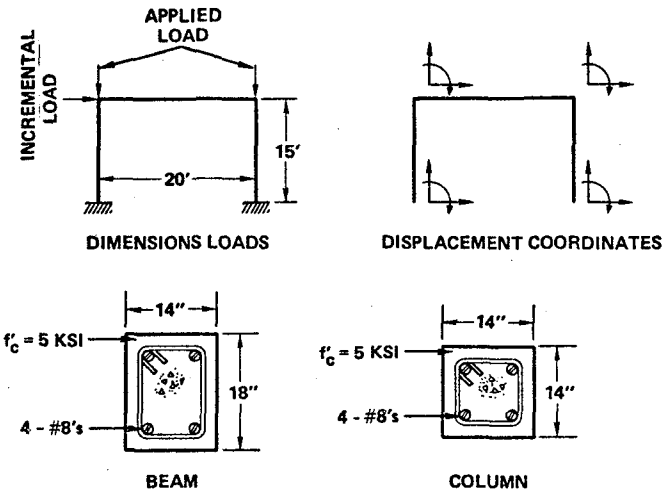

Figure 2. Frame Details.

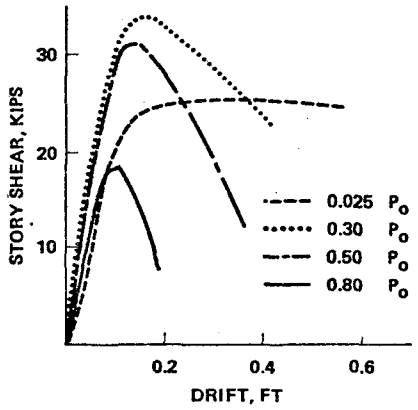

Figure 3. Shear Drift Relations.

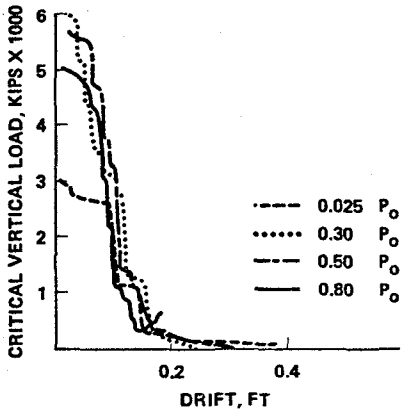

Figure 4. Buckling Load.

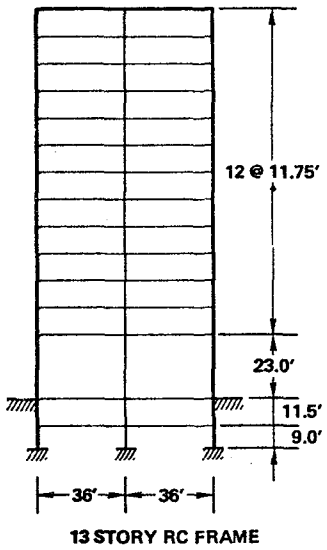

Figure 5. Multistory Frame.

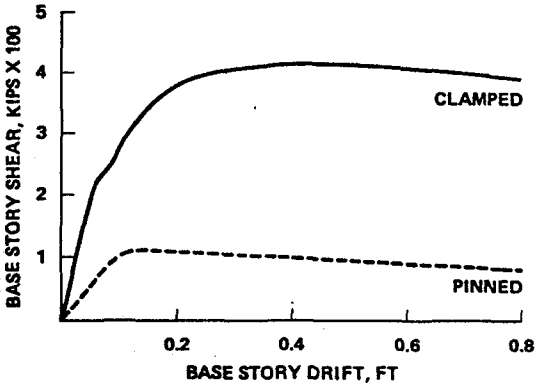

Figure 6. Multistory Frame Shear vs. Drift.

SOIL LIQUEFACTION IN CYCLIC CUBIC TEST APPARATUS

by

William E. Wolfe[I], Mokhtar Annaki[II] and Kenneth L. Lee[III]

INTRODUCTION

Although many studies have been made on soil liquefaction due to cyclic loading, the laboratory tests have always been limited to two directional plane or axisymmetric boundary conditions. In 1967-68, Ko and Scott described a cube type of laboratory device which was capable of subjecting a test specimen to three directional type of normal static stresses (3,4,5). The study described herein used essentially the same equipment, but adapted for cyclic loading liquefaction tests on loose saturated sand.

TEST APPARATUS AND SOIL CONDITIONS

The cubic test apparatus (Fig. 1) consisted of an outer rigid box which held a 4 in cubic sample of soil bounded on all 6 sides by a thin rubber membrane. Thin steel dividers separated these membranes at the edges. Fluid pressure could be applied in the 3 opposing chambers between the rigid box walls and the sample to create the four types of cyclic normal stress illustrated in Fig. 2. Shear stresses could not be applied to the boundary faces.

Approximate cyclic strain measurements were made by noting the amount of water which flowed into or out of the three opposing chambers. Internal pore water pressures were monitored by a thin tube which entered the sample through one corner. The excess pore pressure data were used to define liquefaction failure.

The soil tested was a clean uniform medium subrounded quartz sand known locally as Monterey 20-30 sand, the same sand used by Peacock and Seed (10) (D_{50} = 0.62 mm, C_u = 1.2, e_{max} = 0.85, e_{min} = 0.53). The samples were prepared by wet raining after boiling to saturate and then vibrated to the required density. All tests were performed at 50% relative density where initial liquefaction and large cyclic strains occur almost simultaneously (7).

All samples were isotropically consolidated to σ_c = 15 psi. Symmetrical, uniform cyclic normal stresses were applied at 0.5 Hz. According to the reasoning of Seed and Lee (12), Series A, B and C tests should give the same results. Series D represents a cyclic plane stress test, impossible to simulate in the triaxial apparatus. The large surface area of the sample, and the large grain size caused concern that membrane penetration into the voids at the face might affect the results. This potential problem was partially investigated in Series E and F. Thin brass plates were glued to

---

I Graduate Student, Engr., University of California, Los Angeles.
II Staff Engineer, Woodward-Clyde Consultants, Chicago.
III Professor, Engr., University of California, Los Angeles.

the rubber membranes on the faces subjected to the stress pulsations to reduce the possible membrane penetration effect. For comparison purposes, two sets of cyclic triaxial tests, using 1.4 and 2.8 in dia. samples, were also performed on this sand at the same density and confining pressures as for the cubic sample tests.

The sample response in all series of tests was qualitatively the same as observed from ordinary cyclic triaxial tests on clean loose saturated sand. Transient and permanent pore pressures built up progressively with each cycle to the value of the confining pressure at which point large cyclic strains occurred. The cyclic stress level and the number of cycles required to produce this state of instability was taken as the cyclic strength or initial liquefaction (12) for that test. In general, each test was stopped and the sample dismantled within 5 to 10 cycles after initial liquefaction. For some samples, after the first test, the sample was reconsolidated and retested.

FIRST LOADING CYCLIC LIQUEFACTION TEST RESULTS

The results of all first loading tests in the cube apparatus are shown in Fig. 3. The data indicate no difference between tests with or without plates. The combined data from all cyclic cube tests are shown to the same scale for comparison purposes in Fig. 4a. Data from all but the plane stress Series D tests lead to one fairly well defined curve. Data from Series D form another fairly well defined curve some 40% stronger than the other data.

Initial liquefaction data points from the 1.4 and 2.8 in diam. cyclic triaxial tests showed about the same amount of scatter as the data in any one series of cyclic cubic tests. The best fit strength curves from these cyclic triaxial tests are shown by dashed lines in Fig. 4b. The 2.8 in diam. samples indicated a lower strength than the 1.4 in diam. samples. The cube curves are somewhat steeper than the triaxial curves and intersect the triaxial strength curves. The Series D strength curve is located above both of the cyclic triaxial test curves except for very large numbers of cycles.

No obvious explanation is available concerning the observed variations in cyclic strength with different test conditions. A number of experimental factors may affect the results. Green (2) has criticized the Ko-Scott cube apparatus because of the difficulties at the edges and the corners, which restrict and impede large strains. However, since the pre-liquefaction strains were less than about 1%, the large strain difficiency in the apparatus would not be important. Furthermore, recent comprehensive studies using cyclic triaxial equipment have shown that significant differences in cyclic strength may be obtained from small variations in test procedure (6,9). Nevertheless, the data from all the series of tests, except Series D, were consistent within themselves. This consistency tends to confirm the hypothesis extended from that proposed by Seed and Lee (12) that these three types of tests should give the same results. Although the cube data do not fall directly on the triaxial curves, they are, for all but Series D, sufficiently close to suggest that differences might be due partly to minor experimental apparatus differences and partly to fundamental dif-

ferences in stress patterns.

The observation that Series D test results were significantly stronger than the other Series tests is demonstrated by a fairly large number of tests performed by the first two named writers over a period of about 1 year. Thus, the writers are led to conclude that the cyclic strength in plane stress conditions is significantly greater than in other forms of 3 directional loading.

CYCLIC TESTS ON RECONSOLIDATED SAMPLES

In 1970 Finn, Bransby and Pickering (1) published results of cyclic triaxial tests giving data for first loading liquefaction and for tests on the same samples after reconsolidation. They showed that if the first loading test was stopped before liquefaction occurred, involving cyclic strains less than ± 0.5% single amplitude, then on retesting after reconsolidation the sample would be stronger than measured during first loading tests. Data showing a similar beneficial effect from reconsolidation after previous non-liquefaction cyclic loading were obtained by Lee and Focht (8). Seed et al (13) have also presented similar data from shaking table tests. In contrast, Finn et al (1), found that if the cyclic loading triaxial test was continued beyond initial liquefaction then reconsolidated, an identical cyclic test on the same specimen always caused liquefaction in the first or second cycle, regardless of how many stress cycles were required for liquefaction to occur on the first loading. This observation led Finn et al (1) to suggest that the severe reduction in cyclic strength in reliquefaction tests indicated certain basic changes in the intergranular soil fabric.

Similar results have also been observed by the writers with cyclic triaxial tests. Nevertheless, it was reasoned that this weakening effect must be only a laboratory phenomena and not appropriate for field conditions, otherwise any site which has experienced liquefaction once in the past would reliquefy again at the beginning of every small earthquake. Historical data from Niigata, Japan (11) indicate that this is not the case. It was therefore reasoned that there must be some laboratory influence which produces such an apparent metastable structure after first liquefaction. Possibly this could be due to boundary effect, such as necked samples, which remain after reconsolidation. It could also be caused by internal change in the intergranular packing.

Several reloading tests were performed on the cubic samples after they had first been liquefied. To insure seating after the first liquefaction, the consolidating sample was subjected to 4 stress pulses of the same intensity as the previous test, after which the drain line was closed and the second liquefaction test was performed as usual. During initial liquefaction the volume decreased by about 0.4 to 1.1% corresponding to an average increase in relative density, $D_r < 5\%$. No consolidation volume change was observed as a result of the 4 drained cycles.

The results of the reliquefaction tests are shown in Fig. 5. There is a significant increase in cyclic strength in the reliquefaction tests as compared with the first loading tests. For

reference purposes, a dashed curve has been drawn to show the average strength increase to be expected from a linear increase in relative density of 5%, without any change in interparticle fabric.

Qualitatively, it seems reasonable that if particles bear on each other through sharp asperities, or if large open voids develop during reconsolidation, the soil should be more prone to liquefaction than if the particle contacts were on stronger flat faces and the void distribution was fairly uniform. Small amounts of cyclic loading under drained conditions would wear away sharp and very weak contacts leaving the soil in a more stable structure at essentially the same density. Vibratory compaction in the initial sample preparation should also wear away asperity contacts and lead to a more uniform density distribution than obtained originally by sedimentation from a fluid state. Since these studies were performed, additional comprehensive data by Ladd (6) and Mulilis et al (9) have shown that the cyclic strength of sand may be influenced by as much as 100% by the type of compaction used to prepare test specimens.

In the field, strong earthquake shaking is followed by less intense shaking as part of the same event or as aftershocks. This subsequent shaking should have the tendency of restabilizing the soil following an initial liquefaction so that it would not be as weak as suggested from laboratory tests performed on preliquefied samples without prior drained cyclic loading.

CONCLUSIONS

A limited study has been made on the cyclic liquefaction strength of one loose sand tested in a cubic apparatus and the data compared with data from cyclic triaxial tests. First liquefaction results showed that for all but one of the few possible uniform symmetric normal cyclic stress patterns, the cyclic strengths were the same and were in reasonable agreement with the data from cyclic triaxial tests. For the one cyclic load pattern which simulated a plane stress condition, the cyclic strength was about 40% greater than for the other patterns.

Although samples which have been liquefied and reconsolidated may have a very low resistance to cyclic loading, the reconsolidated cube samples were first subjected to a few cyclic stresses under drained conditions and the apparent metastable structures were destroyed. The samples exhibited greater strength than when first tested. These data along with other recent data suggest that interparticle soil fabric is of considerable importance in the cyclic strength of sands. Field evidence shows that pre-liquefied sand in the field is not as weak as suggested from the laboratory tests performed on pre-liquefied soil without prior drained cyclic stabilization. However, questions still remain unanswered as to what laboratory sample preparation and testing methods are appropriate to simulated field conditions.

REFERENCES

1. Finn, W.D. Liam, Bransby, P.L., and Pickering, D.J. (1970), "Effect of Strain History on Liquefaction of Sand," ASCE, 96,

SM6, 1917-1933.
2. Green, G.E. (1967), "Correspondence on a New Soil Testing Apparatus by Ko, Hon-Yim and Scott, R.F.," Geotechnique, 17, 3, 295.
3. Ko, Hon-Yim and Scott, Ronald F. (1967), "A New Soil Testing Apparatus," Geotechnique, 17, 1, 40-57.
4. Ko, Hon-Yim and Scott, Ronald F. (1968), "Deformation of Sand at Failure," ASCE, 94, SM4, 883-898.
5. Ko, Hon-Yim and Scott, Ronald F. (1968), "Response to Correspondence on a New Soil Testing Apparatus," Geotechnique, 18, 2, 273-274.
6. Ladd, R.S. (1974), "Specimen Preparation and Liquefaction of Sands," ASCE, 100, GT10, 1180-1184.
7. Lee, K.L. and Fitton, J.A. (1969), "Factors Affecting the Cyclic Loading Strength of Soil," ASTM, STP 450, 71-95.
8. Lee, K.L. and Focht, J.A. Jr. (1975), "Liquefaction Potential at the Ekofisk Tank in the North Sea," ASCE, 101, GT1, 1-18.
9. Mulilis, J.P., Chan, C.K. and Seed, H.B., (1975) "The Effect of Method of Sample Preparation on the Cyclic Stress-Strain Behavior of Sands," Report No. EERC 75-18, College of Engineering, University of Calif., Berkeley.
10. Peacock, W.H. and Seed, H.B. (1968), "Sand Liquefaction Under Cyclic Loading Simple Shear Conditions," ASCE, 94, SM3, 689-708.
11. Seed, H.B. and Idriss, I.M. (1971), "A Simplified Procedure For Evaluating Soil Liquefaction Potential," ASCE, 97, SM9, 249-1274.
12. Seed, H.B. and Lee, K.L. (1966), "Liquefaction of Saturated Sands During Cyclic Loading Conditions," ASCE, 92, SM6, 105-134.
13. Seed, H.B., Mori, K. and Chan C.K. (1975), "Influence of Seismic History on the Liquefaction Characteristics of Sands," Report No. 75-25, Collge of Engineering, Univ. of Calif., Berkeley.

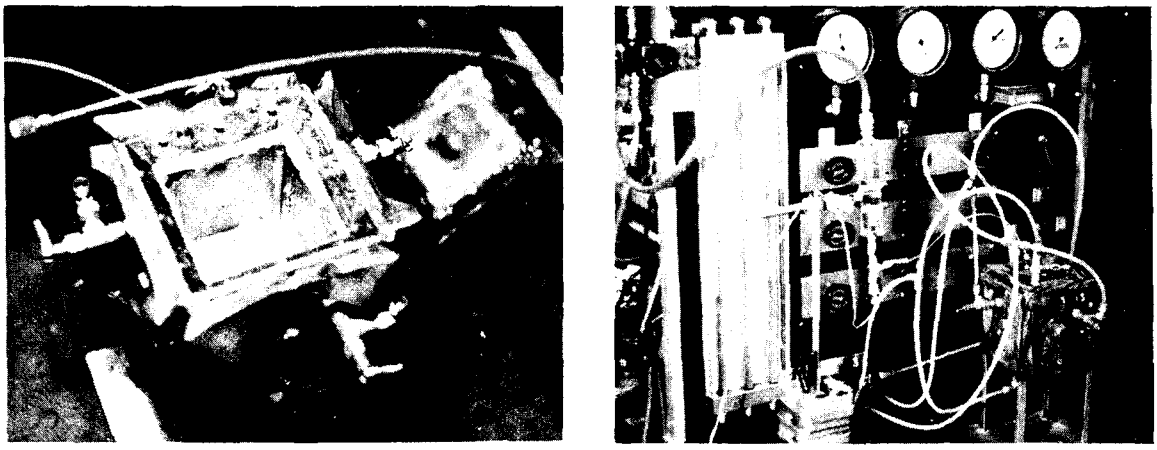

Fig. 1. Photographs of cube cyclic testing apparatus.

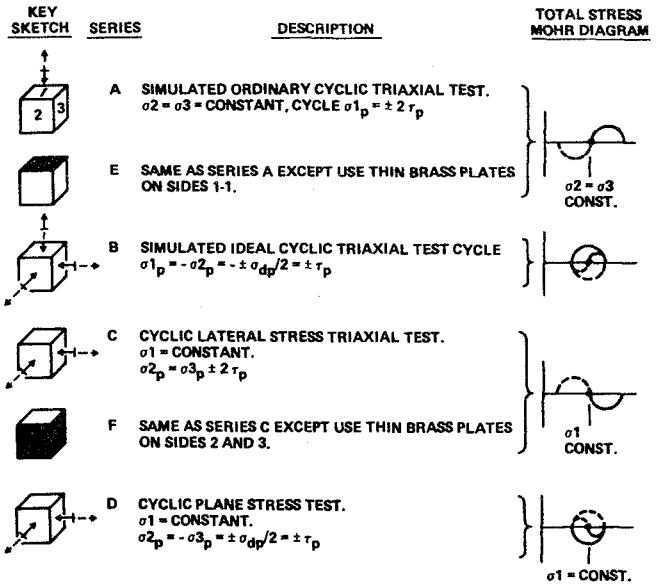

Figure 2. Types of Cyclic Tests Performed on Cubic Samples. All Tests, K_c = 1.0.

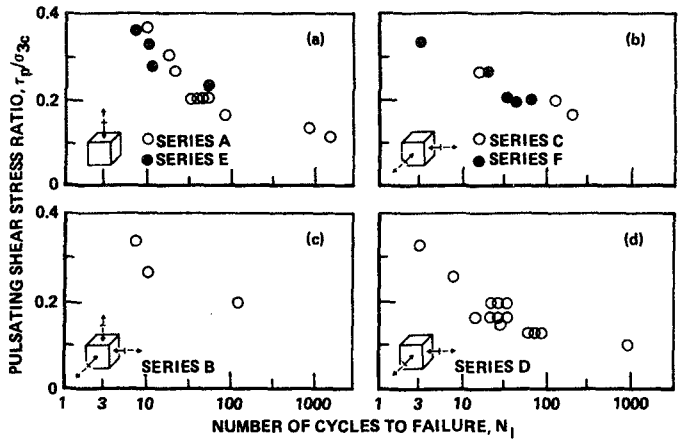

Figure 3. Initial Liquefaction Cycle Strength of Cubic Samples.

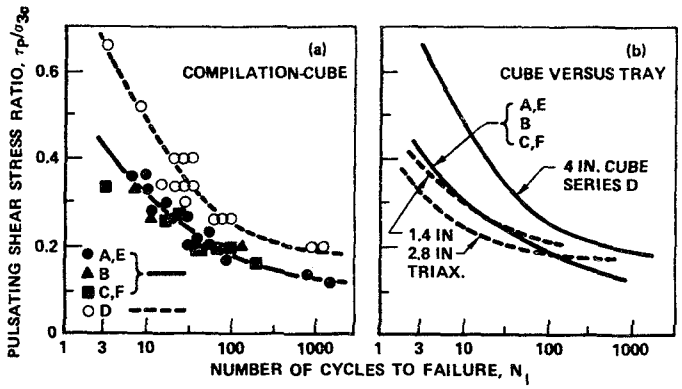

Figure 4. Summary of Initial Liquefaction Cyclic Strength Data.

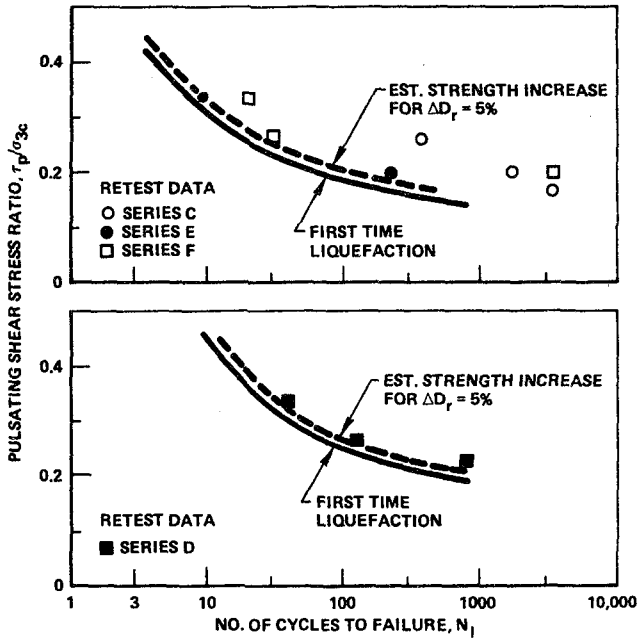

Figure 5. Cyclic Strength After Previous Liquefaction.